JOURNAL OF MATERIALS SCIENCE 24 (1989) 1141–1158

Review
Chemical vapour deposition of superconductors

G. WAHL, F. SCHMADERER
ASEA Brown Boveri, Corporate Research, Eppelheimer Strasse 82, D 6900 Heidelberg, West Germany

Chemical vapour deposition processes (CVD) can produce metastable fine-grained materials as well as epitaxial coatings and can have a very large throwing power depending on the process parameters. Therefore, CVD is an prospective method to deposit high-temperature superconducting materials with $T_c \geqslant 10\,K$. One of the first superconductors which were produced was Nb_3Sn on tapes and single wires. This superconducting material is, however, today produced by metallurgical methods. Since the detection of Nb_3Ge, CVD has become for these coatings the main method of production for the following reasons: high deposition rates, possibility to dope the material by addition of further doping gases to the CVD-process, continuous process. These coatings were deposited on tapes. For the first time the large throwing power of the CVD process was utilized for the deposition of B1-NbC_xN_y on carbon fibre bundles. This opens the possibility to produce multifilamentary structures used for magnetic applications. The structure of the coating can be varied by changing the gas properties, by addition of further gases, by an ultrasonic field, by ignition of a gas discharge and by multi-layering. CVD could also be a prospective method for producing the new class of superconductors with $T_c \geqslant 30\,K$.

1. Introduction

Superconductive materials have many possible applications [1], which can be divided into two different fields.

1. Large-scale applications, mainly high-current applications, e.g. for magnets and for power transmission. Magnets are used as a research tool (e.g. storage rings), for magnetic separation, levitation, nuclear magnetic resonance and for future energy technology such as fusion reactors.

2. The second class of applications are "small scale superconductors" used for microdevices in measurement technology, high-speed computer devices and high-frequency devices.

For all applications, high transition temperatures are desired in order to use small and economic cooling systems. Fig. 1 [2] shows that only a very few superconductors have transition temperatures $T_c \geqslant 10\,K$. The material with the highest superconductivity was for a long time Nb_3Ge with $T_c \sim 23\,K$. Nowadays, new ceramic superconductors of the type Ba–La–Cu–O with a transition temperature $T_c \geqslant 30\,K$ and superconductors of the type RE–Ba–Cu–O (RE = rare earth metals) with $T_c \geqslant 90\,K$ being detected.* Only a very few crystal structures with $T_c \geqslant 10\,K$ exist: A15 compounds, B1-structures, C15 (Laves) phases, Chevrel-phases, K_2NiF_4-type material and perovskites (Table I). A general property of these high-temperature superconductors is their brittleness and, for the A15 and B1 compounds, their low thermodynamic stability.

In addition to the requirement of a high T_c, there is a demand of further optimal properties for special applications: for magnets high current densities at the magnetic field of utilization are necessary. Typical current densities for magnets are in the range of $j_c = 10^5\,A\,cm^{-2}$ (Table I). In order to reach these values, a high critical magnetic field, B_{c2}, and a high critical current density, j_c, are necessary. The B_{c2} is mainly determined by the composition of the superconductor. The critical current density, j_c, is determined by the microstructure, e.g. grain boundaries, precipitates of other materials and crystal faults. Fig. 2 shows the dependence of the critical current density, j_c, at 13 T on the grain size for cubic NbC_xN_y and A15 alloys. In order to reach current densities of $10^5\,A\,cm^{-2}$ for cubic NbC_xN_y, a grain size of 20 nm is necessary; for A15 compounds, however, a grain size of only 0.5 μm is necessary. For magnets the cable must have a multifilament structure in order to obtain electrical and thermal stability [14]. These filaments (diameter $\simeq$ 10–100 μm) must be surrounded by an electrically conducting material like copper (or aluminium) which promotes stability against point disturbances and provides protection against burnout at quench. For the minimization of a.c. losses the filament diameter should be in the range of micrometres.

*An overwhelming number of publications about these superconductors has appeared over recent months; therefore only the primary citations are given here [3, 4]. The newest results are to be found in [5] and the magnetic properties are taken from Okuda *et al.* [6].

0022–2461/89 $03.00 + .12

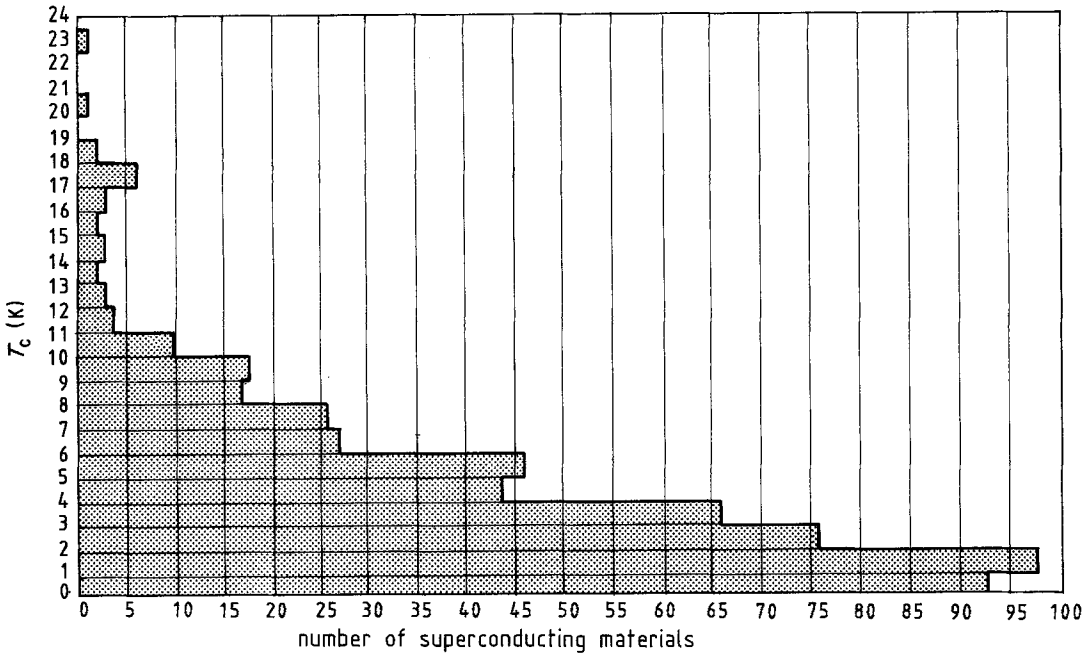

Figure 1 Number of superconducting materials as a function of their transition temperature, T_c [2]. The new ceramic superconductors [3–6] are not included.

For electrical devices which are based on Josephson tunnel junctions, the following properties are demanded [15].

1. Large energy gap Δ. For weak coupling superconductors, Δ varies with the transition temperature, T_c, according to the equation [16] $2\Delta = 3.5kT_c$, where k = Boltzmann constant.

2. A homogeneous material (if possible epitaxial) is required for an abrupt onset of the quasi particle current.

3. Mechanical stability of the layer to thermal cycling.

4. Easy production of a homogeneous insulator layer, if possible by direct oxidation of the superconducting layer.

5. The ratio of junction resistance, R_j, for voltages $U \leqslant \Delta_1 + \Delta_2$ to the resistance R_N for $U \geqslant \Delta_1 + \Delta_2$ should be high. Δ_1, Δ_2 are the energy gaps of the superconducting electrodes.

6. Production of thin layers in the thickness range of micrometres.

2. CVD processes, general remarks

The method of CVD [17–20] belongs to the class of vapour-phase processes where the components which form the coating are transported through the gas phase on to the surface. In contrast to physical vapour deposition (PVD) processes [17], CVD processes always include chemical reactions in the gas phase or on the surface of the substrate, in order to produce the coating

$$A + B \rightarrow C + D \quad (1)$$

where C might be deposited and A, B and D are gaseous components. One necessary condition for CVD is, therefore, that gaseous compounds of the materials to be deposited do exist. There are different possible compounds.

1. Hydrides: e.g. $SiH_4 \rightarrow Si + 2H_2$. This is the basic process for the polysilicon deposition for semiconductor applications.

2. Halogenides: e.g. $TiCl_4 + CH_4 \rightarrow TiC + 4HCl$. This process is used for the production of hard coatings.

TABLE I Superconductive materials

Material	Structure	T_c (K)	B_{c2}(0 K) (T)	B_c(10^5 A cm^{-2}, 4,.2 K) (T)
NbTi	B1	9 [7]	15 [9]	8 [9]
Nb_3Sn	A15	19 [7]	24–26 [9]	15 [11]
Nb_3Al	A15	19 [7]	33 [9]	15 [11]
Nb_3Ge	A15	23 [7]	34–39 [9]	22 [11]
V_3Ga	A15	15 [7]	24 [9]	17 [11]
NbC_xN_y	B1	18 [8]	> 22 [10]	15 [10] (CVD) 20 [11] (sputtered)
$PbMo_6S_8$	Chevrel	14 [8]	60 [9]	2 [11]
V_2(Hf Zr)	Laves	10 [8]	25–28 [9]	5 [11]
$La_{2-x}Sr_xCuO_4$	K_2NiF_4	30 [3–6] > 30	~ 40 [3–6] (anisotropic)	
$Y_1Ba_2Cu_3O_x$	perovskite	90 [3–6]	~ 150 [3–6] (anisotropic)	–

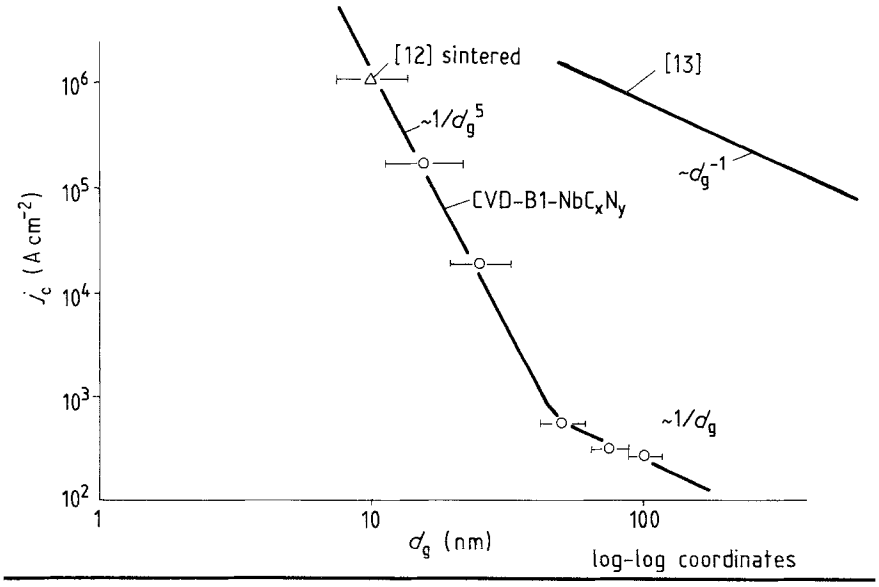

Figure 2 Critical current density at $B = 13$ T plotted against grain size for B1-NbC_xN_y [12] and A15 [13] alloys.

3. Organometallic compounds: CVD with organometallic compounds is used for the production of group II–VI, or group III–V compounds for semiconductor applications, e.g. semiconductor lasers and other optoelectronic applications [21, 22].

In order to produce compounds like oxides, carbides or nitrides, the nonmetallic components are often transported as separate molecules. O_2, CO_2 or H_2O can be used for the formation of oxides, C–H compounds for carbides, NH_3 for nitrides and H_2S for sulphides.

Fig. 3 shows a deposition geometry which is typical for CVD research but nowadays is also important for production facilities. The structure, composition, deposition rate and deposition profile are determined by convection, diffusion, homogeneous and heterogeneous reactions as shown in Fig. 3. Some of the parameters which determine these processes can be reduced to dimensionless groups. The most important group is the Knudsen number $Kn = \lambda/L$ where L is a typical length (e.g. the internal diameter) of the reactor and λ is the mean free path of the gas molecules, which can be estimated by gas kinetical calculations or is tabulated [23]. The value of Kn determines if gas collisions and therefore chemical reactions in the gas phase can be important ($Kn \leqslant 1$) or not ($Kn \geqslant 1$).

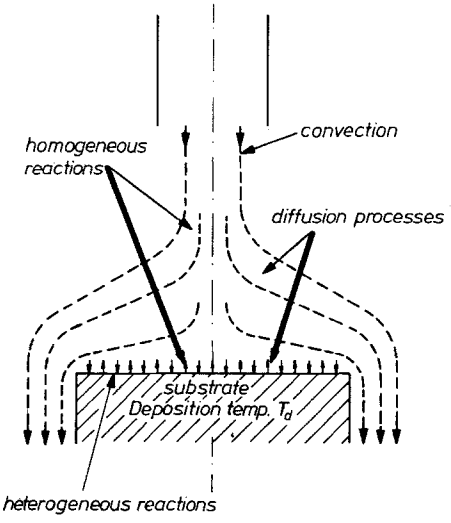

Figure 3 Processes involved in CVD.

The Knudsen number determines, in addition, which kind of theoretical model (continuum theories with or without slip condition, kinetic models) can be used to simulate the deposition process (Fig. 4). For the high-pressure range ($Kn \leqslant 1$) the following dimensionless groups describe the deposition and the gas flow in the reactor [24]:

$$\text{Reynolds number Re} = \varrho_0 v_0 L/\eta_0$$

$$\text{Prandtl number Pr} = \eta_0 C_{p_0}/k_0$$

$$\text{Schmidt number Sc} = \eta_0/\varrho_0 D_{i0}$$

$$\text{Froude number Fr} = v_0^2/gL$$

where η_0 is the viscosity, k_0 the heat conductivity, C_{po} the heat capacity at constant pressure, D_{io} a diffusion constant of component i, g gravity, ϱ_0 the mass density, v_0 typical gas velocity in the reactor. The gas flow in a stagnation flow reactor is shown in Figs 5, 6 where the influence of gravity on the gas flow is demonstrated. Many simulation calculations of the gas flow have been carried out in recent years [24–28]. Typical deposition temperatures for CVD processes are given in Fig. 7. As shown, CVD depositions take place over a large range of temperatures from 400 K (deposition of oxides from alkoholates) to 1800 K (deposition of ceramics from chlorides). In this figure, particular emphasis has been put on CVD processes for superconductors. Details of these processes will be described in the following sections.

The mass deposition rate, $\dot{m}$, is described by the Sherwood number

$$Sh = \dot{m}L/DY_0\varrho_0$$

which depends on the parameters mentioned

$$Sh = f(r^*, Re, Sc, Pr, Fr, \ldots) \qquad (2)$$

where r^* is the dimensionless coordinate on the substrate and Y_0 a typical mass fraction in the reactor.

In addition to the numbers given in parentheses, the deposition also depends on chemical reaction constants, and on numbers which describe the temperature and concentration dependence of the gas properties.

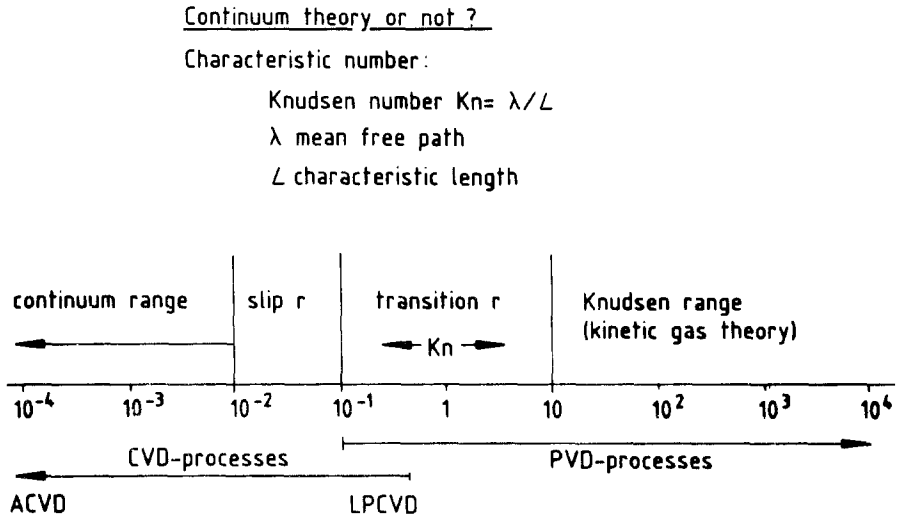

Figure 4 Classification of gas-phase processes according to the Knudsen number, Kn ACVD = chemical vapour deposition at atmospheric pressure, LPCVD = low-pressure CVD, PVD = physical vapour deposition.

Re, Sc, Pr, Fr are mostly calculated by the inlet properties of the gas. The maximum achievable deposition rate produced by CVD depends on the mass transport in the gas phase and can reach values of $\sim 100\,\mu m\,min^{-1}$ as was obtained, e.g. at the tungsten deposition from WF_6 and H_2 [30]. A characteristic quantity determining the structure and phase of the deposited material is the free enthalpy difference, ΔG_{gs}, between the gas phase and the condensed phase. ΔG_{gs} can be estimated in the following way.

From the measured molar deposition rate, j_d, an effective concentration, n_{eff}, above the coating can be estimated from [31]

$$j_d = n_{eff} v/4 \quad (3)$$

where v is the mean thermal velocity of the molecules in the gas phase. The free enthalpy difference, ΔG_{gs}, is given by

$$\Delta G_{gs} = RT_d \ln (n_{eq}/n_{eff}) \quad (4)$$

where n_{eq} is the equilibrium concentration of the deposited material at the substrate temperature, T_d. Table II shows for nickel and niobium at typical molar deposition rates j_d, the free enthalpy changes at different deposition temperatures. The concentrations n_{eff} and n_{eq} and the partical pressures p_{eq} and p_{eff} given in Table II are correlated by the relations $n.. = p../kT_d$, (where k is the Boltzmann constant.) This table shows that the free enthalpy difference, ΔG_{gs}, is so large that metastable phases, amorphous or fine-grained structures can be formed, because typical free-enthalpy changes from one condensed phase to another are in the range of $kJ\,mol^{-1}$: in order to give an impression of these values, the free-enthalpy difference, ΔG_{sl} between the solid phase and the liquid phase are given in Table II. As can be seen, the absolute values, ΔG_{sl}, are much smaller than ΔG_{gs}. Therefore, the CVD process is a candidate for the formation of metastable phases, amorphous or fine-grained structures and is in competition with other methods like physical vapour deposition, liquid quenching and laser treatment. The phases really formed by CVD processes depend additionally on the growth kinetics, which are determined by the deposition parameters.

The possibility to deposit these different phases or structures by CVD, makes this process interesting

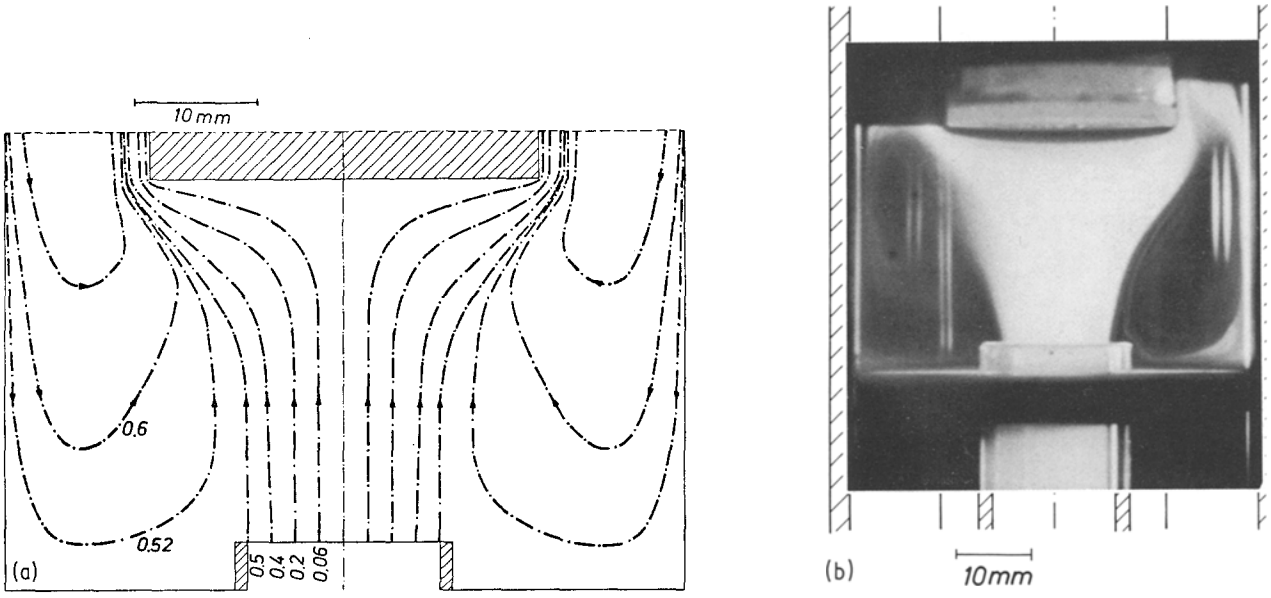

Figure 5 (a) Calculated and measured (TiO_2–fume) stream lines in a stagnation flow reactor [24]. (b) Deposition surface *above* the gas inlet showing the flow pattern: Re = 50, Fr = 0.09, ΔT = 600° C, N_2.

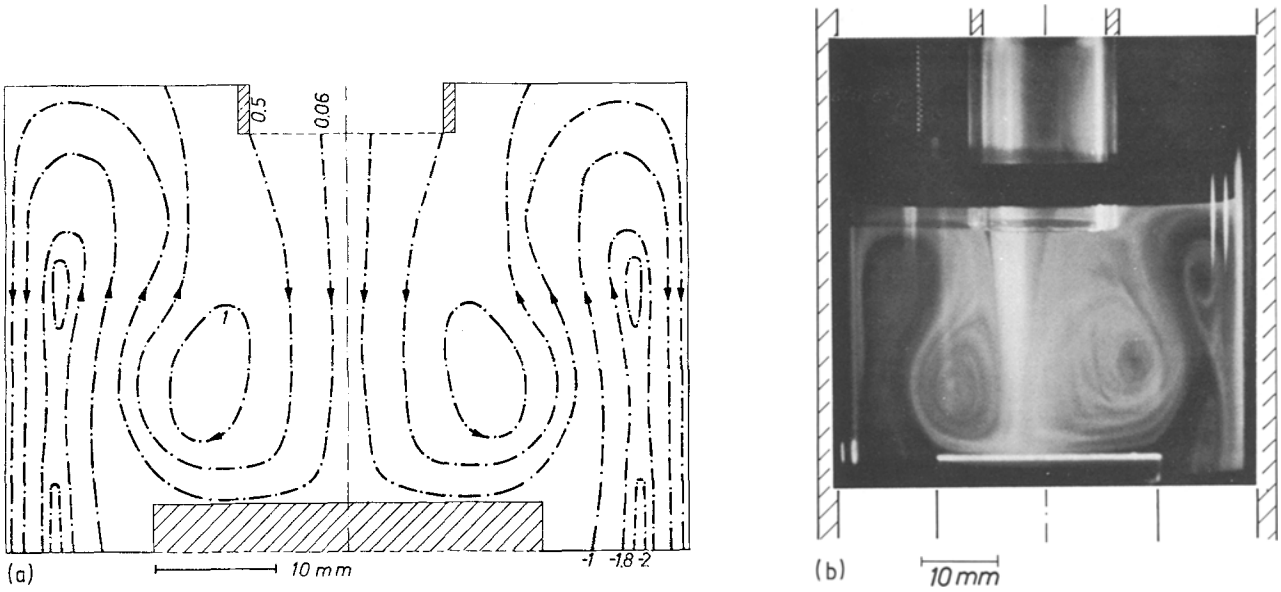

Figure 6 (a) Calculated measured (TiO_2-fume) stream lines in a stagnation flow reactor [24]. (b) Deposition surface *below* the gas inlet, showing the flow pattern: Re = 50, Fr = 0.09, ΔT = 600° C, N_2 [24].

for deposition of superconducting materials. Another reason is the large throwing power of CVD, in comparison to PVD processes. It is therefore possible to deposit multifilament structures as shown in Section 3.2.

For almost all CVD experiments of superconductors the chloride process (chloride + H_2 → alloy + HCl) is used as indicated in Fig. 7. Only very recently have there been considerations to apply CVD with metal-organic compounds (NbN [34], A15 [35] $YBa_2Cu_3O_x$ [36]). These processes work at lower temperatures and the gas phase is more unstable; therefore, the preparation of more thermodynamically unstable structures should be possible.

3. CVD of superconductors

3.1. CVD of A15 superconductors on tapes and single wires

3.1.1. CVD of Nb_3Ge

The first known CVD process for the production of superconductors was the deposition of Nb_3Sn according to the reaction

$$H_2 + \text{Nb chloride} + \text{Sn chloride} \rightarrow Nb_3Sn + \ldots \quad (5)$$

With this process it was possible to coat tapes ([37, 38, 39, 40]). Today, however, the main stream of the development of Nb_3Sn is concerned with solid state diffusion processes (a metallurgical technique).

CVD processes for superconducting Nb_3Ge became very attractive because different groups [41–43] produced Nb_3Ge with the transition temperatures of $T_c \geqslant 20$ K which compared very well with value of T_c = 22.3 K, found with sputtered layers [44]. The following CVD process was used

$$6NbCl_5 + 2GeCl_4 + 19H_2 \rightarrow 2Nb_3Ge + 38\,HCl \quad (6)$$

This CVD process was used to deposit discontinuously on samples and continuously on ribbons or single wires (Figs 8a, b). Table III shows the deposition rates on ribbons with the chloride process and the properties of the layers.

The reaction gas can be produced either by direct chlorination of niobium and germanium in a Cl_2 or HCl gas flow (as in Fig. 8a) or by direct evaporation of $NbCl_5$ and $GeCl_4$. The direct chlorination has in comparison to the evaporation technique, the following advantages.

1. The impurity content of the chlorides produced by direct chlorination can be lower than with evaporated chlorides [53].

2. By changing the chlorination conditions, different chlorides $NbCl_x$ and $GeCl_y$ can be produced:

TABLE II Free transition enthalpy differences, ΔG_{gs}, between vapour and coating in comparison to free transition enthalpies, ΔG_{sl}, in the condensed phase (liquid–solid)

Metal	M ($g\,mol^{-1}$)	T_d (K)	P_{eq} (Pa) [32]	j_d ($mol\,cm^{-2}\,sec^{-1}$)	P_{eff} (Pa)	ΔG_{gs} ($kJ\,mol^{-1}$)	ΔG_{sl} ($kJ\,mol^{-1}$)
Ni	57	1000	1.24×10^{-5}	10^{-4}	1.74	−99.1	+6*
				10^{-5}	0.174	−79.830	
				10^{-6}	0.0194	−60.56	
Nb	92.9	1300	3.99×10^{-20}*	10^{-4}	2.52	−495.5	+5*
				10^{-5}	0.252	−470.5	
				10^{-6}	0.0252	−445.4	

*Linearly extrapolated values [33].

M, molar mass; T_d, deposition temperature; P_{eq}, equilibrium partial pressure of the metal atoms at deposition temperature T_d; j_d, molar deposition rate; P_{eff}, effective partial pressure.

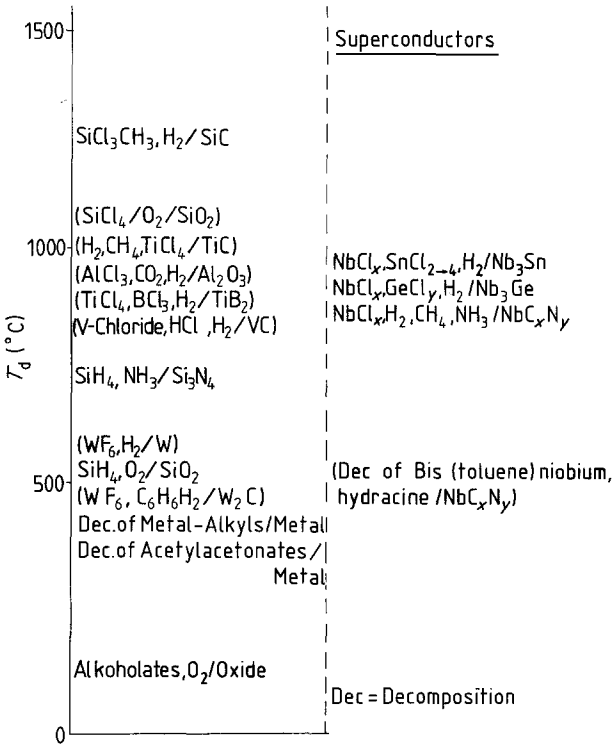

Figure 7 Deposition temperatures for CVD processes. The gas mixture is given before the solidus and the deposition product after it.

$x = 4$ at $T \geqslant 1200°C$, $x = 4$ to 5 at $T = 600$ K [54], $y = 4$, $T \leqslant 700$ K, $y = 2$, $T \geqslant 700$ K [54]. Similar effects of changing the stoichiometry of $NbCl_x$ with chlorination conditions was also found at the Nb_3Ga deposition [55].

The CVD process and the dependence of the layer structure on the deposition parameters has been thoroughly investigated by Weiss *et al.* [45]. The deposition geometry used for these experiments is shown in Fig. 8a. The following parameters determine the deposition process: deposition temperature T_d, the chlorination temperature T_{Nb} and T_{Ge} of niobium and germanium, the total pressure p, the chloride ratio

$$g = \frac{i_{Cl_2}(Nb)}{i_{Cl_2}(Nb) + i_{Cl_2}(Ge)} \quad (7)$$

the dilution parameters

$$d_1 = i_{Ar}/i_{Cl_2}(Nb), \quad d_2 = i_{Ar}/i_{Cl_2}(Ge), \quad d_3 = i_{Ar}/i_{H_2} \quad (8)$$

and the reduction parameter

$$r = i_{H_2}/[i_{Cl_2}(Nb) + i_{Cl_2}(Ge)] \quad (9)$$

$i_{Cl_2}(Nb)$ and $i_{Cl_2}(Ge)$ being the gas flow through niobium and germanium, i_{Ar} and i_{H_2} the total gas flow of argon and hydrogen.

Fig. 9 shows the measured phases and Fig. 10 the calculated boundaries of the different phase areas in dependence on T_d and g. Both figures show a good agreement of measurement and calculation. The thermodynamic calculations are based on a minimization of the Gibbs free energy including the condensed material [45]. Fig. 11 shows the T_c value plotted against g. The comparison of Figs 9, 10 and 11 shows that the maximum T_c values are reached in the two-phase range [45].

In addition to optimizing T_c, optimal values of j_c and B_{c_2} must be reached. In the following paragraphs some important influencing parameters are discussed.

1. Influence of Nb_5Ge_3. Different research groups [48, 56–58] have observed that a fluxoid pinning in Nb_3Ge occurs by dispersed nonsuperconducting particles like tetragonal Nb_5Ge_3. The plot of the critical current j_c at $13.8\,T$ against the weight content of Nb_5Ge_3 deposited at 875° C on tape material [48] shows a maximum j_c at 3 wt % Nb_5Ge_3 and at high content a decrease of j_c. The position of the peak depends on the deposition temperature (Fig. 12) [48].

2. Influence of doping material. In an early study of Nb_3Sn prepared by CVD, Enstrom and co-workers [59, 60] observed an enhancement of j_c by addition of impurities which form a second phase. They attributed this enhancement to pinning on grain and subgrain boundaries. In contrast, Ziegler *et al.* [61] and Uzel and Diepers [62] suggested that pinning occurs on a network of intragranular defects associated with the precipitated carbon or carbide particles. Braginski *et al.* [63] investigated the influence of N_2, C_2H_6 or CO_2 on the superconducting properties of Nb_3Ge. Fig. 13 shows the critical temperature plotted against the impurity content in the layer where the N_2 is bound in the form of fine dispersed particles (30 nm) of NbN and C in the form of NbC. Doping with CO_2 produces a remarkable lowering of T_c (Fig. 13) which is correlated with the incorporation of oxygen rather than carbon [63]. With carbides and nitrides an increase of the critical current density to a maximum value and then a decrease (Fig. 14) was found. The comparison of j_c values with the microstructure investigated by TEM, has shown that predominant flux pinning occurs on carbides and nitrides incorporated in Nb–Ge layers [63].

TABLE III CVD Nb_3Ge coatings on tapes or single filament, deposition parameters and layer properties

Material	Substrate	Velocity of the ribbon ($m\,h^{-1}$)	Thickness of the layer (μm)	T_c (K)	Critical current density ($A\,cm^{-2}$)	
Nb_3Ge	Nb-filaments coated with W-1% ThO_2	4	7–14	18		[47]
Nb_3Ge	stainless steel 4 mm × 12 μm		3–4	$\leqslant 20$	10^4 20 T, 4.2 K	[46]
Nb_3Ge	Ni, Cu stainless steel coated with Cu	2–4	3–6	17–19	1–2.5 13.8 K	[48]
Nb_3Ge	stainless steel 3 mm × 0.05 mm	20	a few μm	> 20	7.7×10^4 15 T, 4.2 K	[49, 50]
Nb_3Ge	Hastelloy 2 mm × 50 μm	18	a few μm	17–19	$1.5–6 \times 10^5$ 5 T, 4.2 K	[51, 52]

Deposition of Nb_3Ge on ribbons and single filaments.

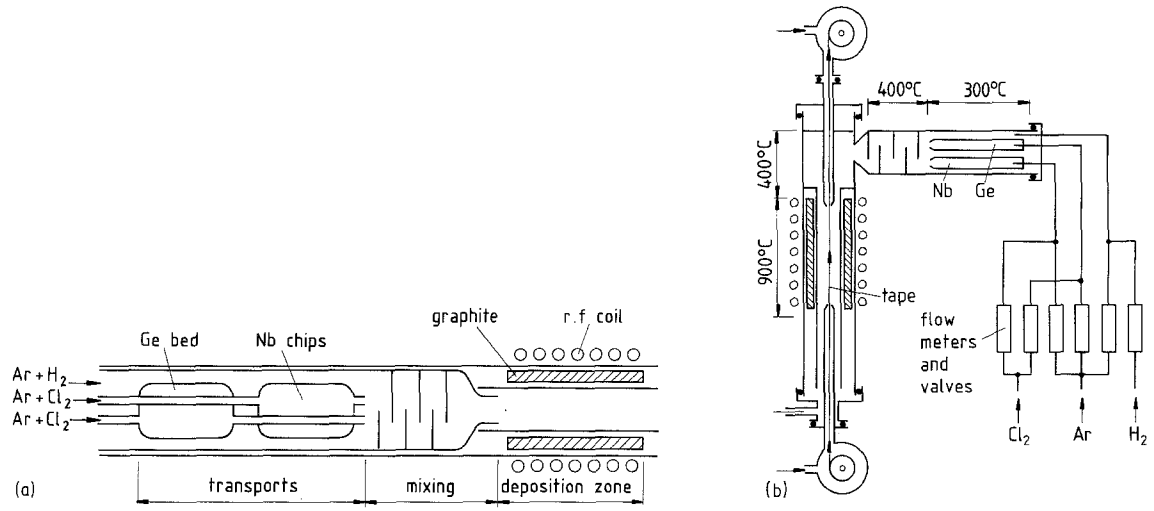

Figure 8 (a) Schematic view of a CVD reactor with direct chlorination [45]. (b) CVD apparatus for the coating of superconducting tapes [46] with direct chlorination of niobium.

3. Studies by Braginski *et al.* [64] and by Kampwirth [65] have shown a strong decrease of j_c with increasing film thickness, caused by larger grains in the thicker films. The same phenomenon was observed by Maley *et al.* [48]. Braginski has avoided this grain growth in thicker films by a multilayer structure of Nb_3Ge layers ($\sim 1.5\,\mu m$ thick), with ~ 100 nm thick diffusion layers of iron or iron oxide [64]. The formation of interlayers, especially metallic interlayers, can have basically two effects: (1) providing a finer grain structure and (2) the normal metal itself can provide pinning sites. Maley *et al.* [66] obtained multilayering by varying the process parameters. Every 2 min at 30 sec intervals the rate of germanium delivery was reduced to create germanium-deficient regions between layers of high T_c–Nb_3Ge. Thus superconducting layers with a thickness of ~ 950 nm separated by germanium-deficient layers (300 nm) were produced. The measurement of j_c did not, however, in this case show an enhancement of the critical current. An explanation of this phenomenon cannot be given [66].

4. Modification of the substrate. As was shown by Ekin [67] A15 compounds are stress sensitive. In CVD processes stresses are induced by the different thermal expansion coefficients between substrate and superconductor. The resulting stress values are calculated for different substrate materials (Table IV) whereby for Nb_3Ge a thermal expansion coefficient of $6.98 \times 10^{-6}\,K^{-1}$ was assumed [48]. According to Maley *et al.* [48] the temperature dependence of j_c can be described (Fig. 15) by

$$j_c = j_{co}[1 - (T/T_c^*)^2] \qquad (10)$$

where T_c^* is a material-dependent parameter generally

TABLE IV Compression and T_c^* at Nb_3Ge coatings [48]

Substrate	Compression (%)	T_c^* (K)
Nickel	0.95	12–13
Stainless steel (400 series)	0.53	12.5
Steel (1015)	0.52	12.5
Niobium	0.11	17.5–18.0
Niobium–1% Zr	0.08	18.0
Tantalum	0.02	18–19

a few degrees below the inductively measured T_c. The stress decreases T_c^* as is shown in Fig. 16, where the values resulting from coatings on different substrate materials (Table IV) are plotted against the compressive stress.

5. Modification of Nb_3Ge. In order to increase the stability, i.e. to increase T_c, ternary alloys of the system Nb–Ge–Ga were deposited, where $GaCl_3$ was produced by direct chlorination of gallium metal housed in a quartz-lined nickel chamber maintained at 500° C. Fig. 17 shows the dependence of the lattice spacing and the critical temperature on the ratio Ga/(Ga + Ge) [48]. Ternary superconductors based on Nb–Ge–Sn [68] were prepared by direct chlorination of Nb–Ge–Sn–Alloys at 700° C. The superconductors were deposited on Al_2O_3, niobium, molybdenum, copper, Be_2O_3 and $LiNbO_3$. With a constant niobium content in the layer, the dependence of T_c on Sn/(Ge + Sn) shows a minimum value of T_c. At Ge/Sn = 1, a critical temperature of $T_c = 14$ K was found.

Alterowitz *et al.* [69] measured the influence of tin on

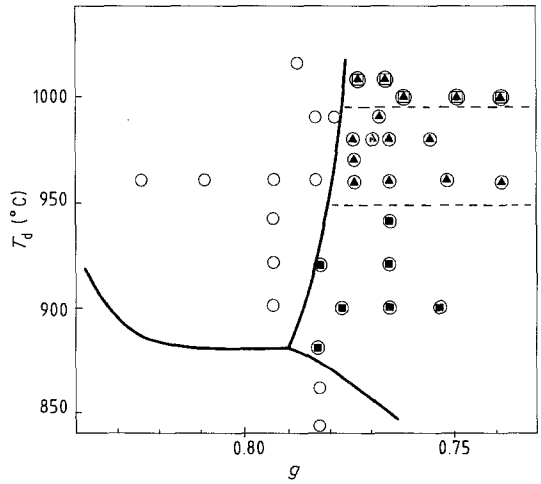

Figure 9 Experimental CVD-phase diagram with deposition temperature, T_d, and chloride ratio, g, as independent variables [45]. T_2, H_2, H_1 are different Nb_5Ge_3 phases discussed in detail in [45]. $T_{Nb} = T_{Ge} = 300$° C; $\Sigma Cl = 40\,ml\,min^{-1}$; $d_1 = 10$, $d_2 = 20$, $d_3 = 0$, $r = 20$. (○) Nb_3Ge; (■) T_2-, (▲) H_2-, (□) H_2-Nb_5-Ge_3.

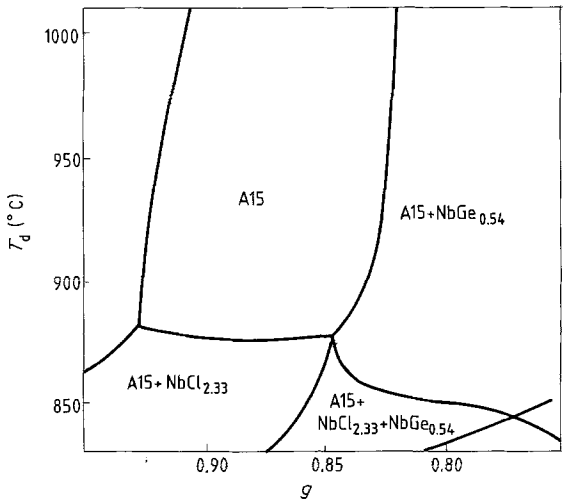

Figure 10 Computed CVD-phase diagram for the A15 phase with T_d and g as independent variables [45]. $d_1 = 10$, $d_2 = 20$, $d_3 = 0$, $r = 20$, $T_{Nb} = T_{Ge} = 327°C$.

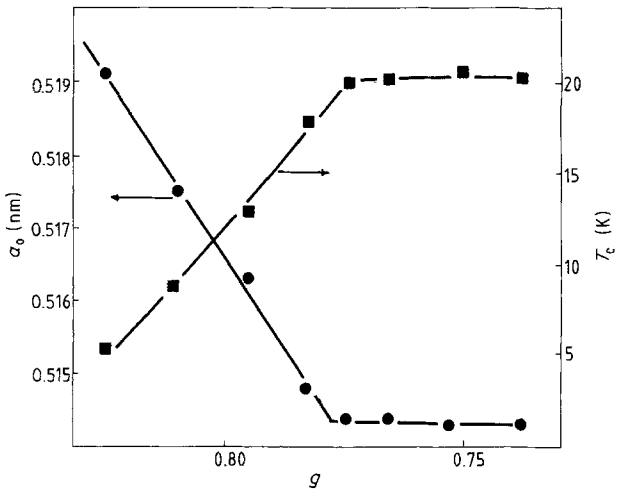

Figure 11 Variation of the A15 cubic unit cell parameter and of the T_c-midpoint with the chloride ratio g at $T_d = 960°C$ [45].

the critical field B_{c2}. They found a minimum value of B_{c2} in the compound $Nb_3Ge_{1-x}Sn_x$ with $x = 0.4$.

3.1.2. Other A15 superconductors

Table V shows important parameters found with Nb_3Ga, Nb_3Si, V_3Si and compares the properties found by CVD deposition to those found with other methods.

3.1.3. General remarks on the deposition of A15 compounds

Fig. 18 summarizes typical j_c–B curves of different advanced superconductors, produced by different methods. Large values of j_c for generating fields of over 20 T have already been obtained with Nb_3Ge tapes. The next step in the research of CVD is to develop filament-structured wires. This was done for the first time by Braginski *et al.* [80] who deposited Nb_3Ge by CVD on 200 Al_2O_3 fibres (20 μm diameter). But the main development of the fibre production is in the field of NbC_xN_y deposition, described in the next section.

3.2. CVD of B1-superconductors on fibres

3.2.1. General remarks about B1-superconductors

The other group of superconductors besides A15 compounds, produced by CVD are carbides and nitrides which have a B1 structure. For superconducting investigations HfN, TiN, ZrN [81] and NbN were deposited by CVD. Fig. 19 shows the transition temperatures of carbides and nitrides plotted against the valence electron density which, according to You-xian and Shou-an [82], should be a characteristic parameter for the superconductivity of these compounds. The corresponding carbides and nitrides are always connected for clarification by straight lines.

According to Fig. 19, NbN has the highest measured T_c value in this group, only the suggested value of MoN may be higher. The T_c range of MoN is extrapolated with the help of the slopes of the straight lines between the corresponding carbides and nitrides in Fig. 19. The high value of T_c of MoN, however, has not been verified experimentally [83]. One reason could be the high value $\lambda = 1.58$ of the electron–phonon coupling constant λ [84]. Both the high λ and high T_c suggest [84] that B1-MoN probably lies beyond the phase boundary of stability for the B1-structure compounds, as is the case in the large λ-region of many phases [85, 86].

The most interesting material for applications is NbN, for the following reasons.

1. B1-niobium nitride has a high T_c (Fig. 19).
2. B1-niobium nitrides are not sensitive to radiation [87]. Therefore B1-NbC_xN_y can be used for fusion applications.
3. B1-niobium nitrides, in contrast to other superconductors like A15-alloys and NbTi [67, 88], are not sensitive to strain [89]. In Nb_3Sn, a 0.4% intrinsic strain results in a 60% degradation of the critical current density, j_c, at 16 T, whereby the strain effect increases at higher fields. Niobium nitride shows no degradation in the measured range of the magnetic induction $B \leqslant 22$ T and strain $\varepsilon \leqslant 0.7\%$. B1-niobium nitrides are therefore suitable for high magnetic fields.

A strong limitation for the production of NbN is the stability of the B1-phase only at temperatures $\geqslant 1300°C$ (Fig. 20). However, as is shown in Fig. 20, the cubic phase can be stabilized at lower

TABLE V A15-superconductors made by CVD (except Nb_3Sn and Nb_3Ge)

Superconductor	CVD-gas mixture	T_d (°C)	T_c (CVD) (K)	Ref.	T_c, any method	Ref.
Nb_3Si	$NbCl_5$, $SiCl_4$, H_2	800–900	4.3– 8	[70]	18.5–19	[8, 73]
V_3Si	VCl_4, $SiCl_4$, H_2	990	14.8–16.7	[71]	16.9	[8]
Nb_3Ga	$NbCl_5$, $GaCl_3$, H_2	700	20.3	[41, 72]	20.7	[8]

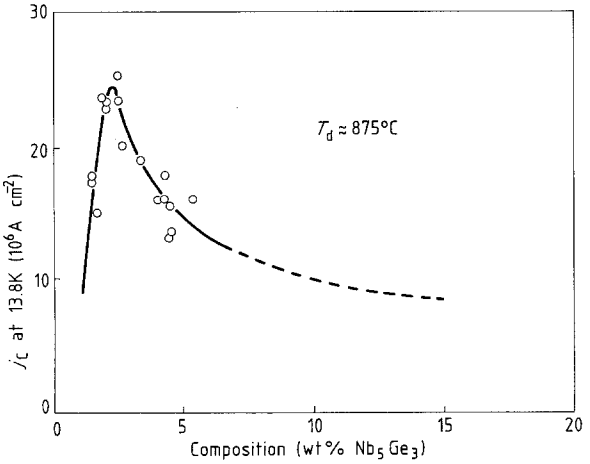

Figure 12 j_c (13.8 K) plotted against composition (wt % Nb_5Ge_3) [48].

temperatures by carbon addition. This carbon addition has a further advantage: the critical temperature T_c can be increased. Hulm and co-workers [94, 95] and Williams *et al.* [96] have found for B1-$NbC_{0.3}N_{0.7}$ a maximum T_c = 17.8 K (compared to T_c = 15 K [94] to 17.3 K [96] for B1-NbN). This maximum is found in accordance with the Matthias rule [97, 98] at a valence electron density of 4.7 electrons/atom. The cubic phase can also be stabilized by low concentrations of oxygen [99].

The deposition of stabilized B1-NbN layers was carried out by sputtering and by CVD processes. Reactive sputtering B1-NbN layers on sapphire, graphite, alumina or Hastelloy produced very high self-field current densities ($\geqslant 10^7$ A cm^{-2}) and very high critical magnetic fields B_{c2} = 20 to 50 T [100]. These properties were measured on very thin layers (50 nm) having a columnar void-structure (grain size ~ 10 nm). Applications of this coating process for fibre bundles are discussed by Dietrich *et al.* [101].

In the following sections the depositions of carbon-stabilized B1-NbN by CVD on fibre bundles is discussed.

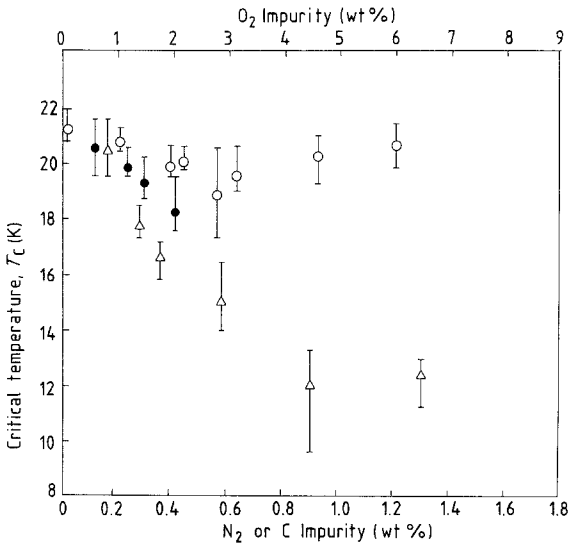

Figure 13 Critical temperature (midpoint) plotted against concentration of N_2/C in the Nb_3Ge layers [63]. The dopant gas is given at the measuring points: (○) NbN (N_2), (●) NbC (C_2H_6), (△) O_2 (CO_2).

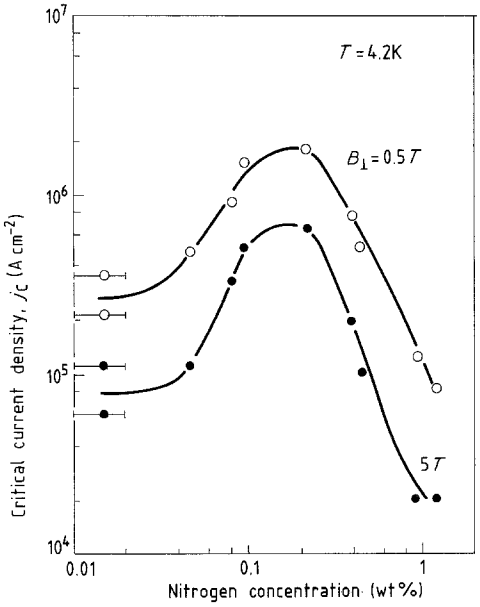

Figure 14 Critical current density plotted against nitrogen concentration in N_2-doped samples [63] for two different magnetic fields H, which are perpendicular to the layer surface.

3.2.2. CVD of NbC_xN_y on carbon fibres

For the deposition of carbon-stabilized niobium nitride (NbC_xN_y), carbon fibres were used for the following reasons.

1. High-temperature resistance of the carbon fibre.
2. High elastic modulus, which protects the brittle superconducting coating.
3. High tensile strength.
4. Availability in a variety of modifications (therefore easy modification of the surface properties).

The simplest deposition process of carbon-stabilized niobium nitride is the chloride process

$$NbCl_5 + 5/2\,H_2 + yNH_3 + xCH_4 \rightarrow NbC_xN_y + \ldots \; T \geqslant 900°C \qquad (11)$$

Unfortunately this one-step process [102] results in low critical magnetic field values of about 12 T [103, 104] and low critical current densities [93]. The main

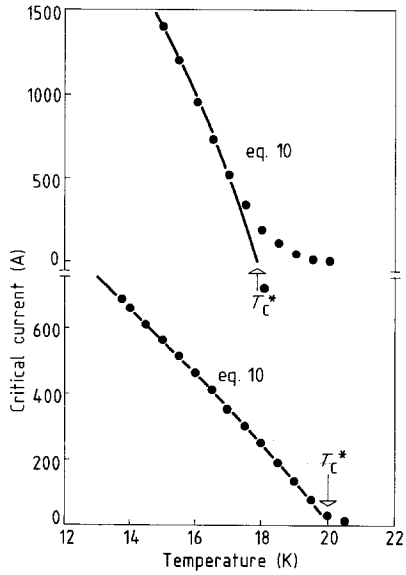

Figure 15 Plots [48] of critical currents against temperature for two Nb_3Ge samples and the description of $j_c(T_c)$ by Equation 10.

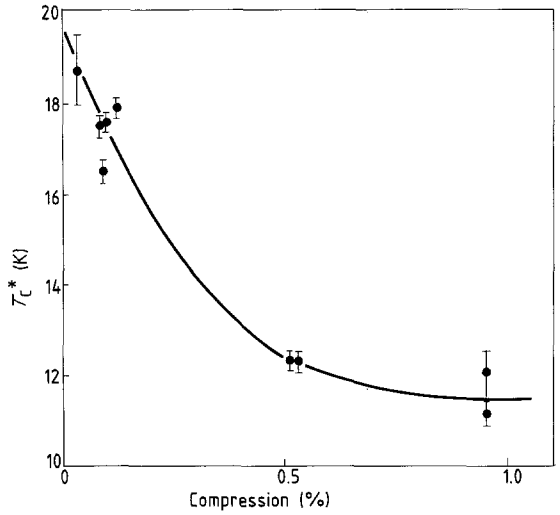

Figure 16 T_c^* plotted against compression (Table IV) for Nb_3Ge coatings [48].

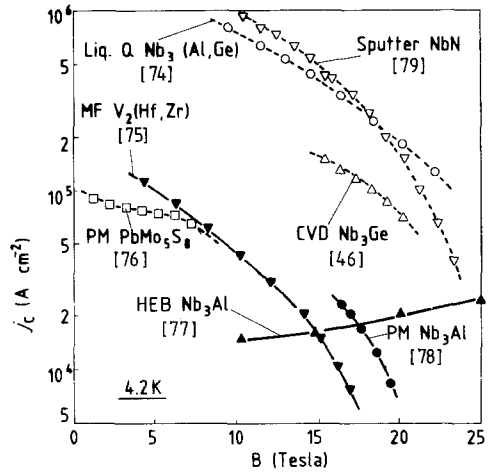

Figure 18 j_c–B curves for different kind of specimens. Solid lines and symbols (▲, ●) show j_c for overall area, without the copper-stabilization and dashed lines and symbols (△, ○, □) show j_c only for the compound area. PM = powder metallurgical processes; Liq. Q. liquid quenching; MF = multifilamentary wires, cold drawn and reacted, HEB = high electron beam irradiation.

disadvantage of the one-step process (Reaction 11) is that the crystal structure, the composition and the microstructure cannot be optimized independently; therefore, a two-step process was proposed [105–107]. In the first step the mainly hexagonal NbN_ε-phase ($\varepsilon \leqslant 1$) is deposited according to the reaction

$$NbCl_5 + 5/2\,H_2 + 1/2\,\varepsilon N_2 \rightarrow \text{hex. } NbN_\varepsilon + \ldots \quad (12)$$

In this step the microstructure can be optimized. In a second step the B1-phase is generated

$$NbN + xCH_4 + (y - \varepsilon)\,NH_3 \rightarrow \text{B1-}NbC_xN_y + \ldots \quad (13)$$

Two experimental arrangements were constructed to coat fibres using the two-step process: one for atmospheric pressure [105–108] and a second for both low-pressure CVD (LPCVD) and atmospheric pressure CVD [108, 109].

The following considerations concentrate on LPCVD (1) the throwing power is large in LPCVD [105]; (2) the dust formation was found to be lower in LPCVD, therefore the chemical engineering is less complicated [105].

Fig. 21 shows the apparatus [108, 109] used for the LPCVD deposition. The gas flow in the different reactors I, II, III and the movement of the fibre bundle are indicated in Fig. 21. The leakage rate of the whole apparatus was smaller than $3.10^{-4}\,l\,h^{-1}$ (STP). The gas flow in all resistance-heated reactors is separated by baffles between the reactors. The reactors are constructed from quartz, the tubing in the room-temperature region and the $NbCl_5$ evaporator are made of stainless steel. Reactor 1 was used to remove the organic finish from the carbon fibres and to optimize the surface activity by annealing in a controlled atmosphere (N_2). In the second reactor, NbN_ε was deposited (Reaction 12) and in the last reactor, the carbonitriding process (Reaction 13) was carried out at temperatures $\geqslant 1050°\,C$ in order to obtain the B1-NbC_xN_y-phase. The standard deposition conditions were: reactor I, $T_1 = 1000°\,C$, $i_{N_2} = 12\,l\,h^{-1}$ (STP); reactor II, $T_2 = 900°\,C$, $i_{H_2} = i_{N_2} = 10\,l\,h^{-1}$ (STP); reactor III, $T_3 = 1100°\,C$, $i_{CH_3} = i_{NH_4} = 10\,l\,h^{-1}$ (STP), where T_i are the temperatures in the quartz reactors, i = I, II, III, $i_{..}$ are the corresponding gas flows of the components indicated by the subscripts. Other deposition conditions are: evaporation temperature of $NbCl_5$, $T_{NbCl_5} = 110°\,C$; total pressure,

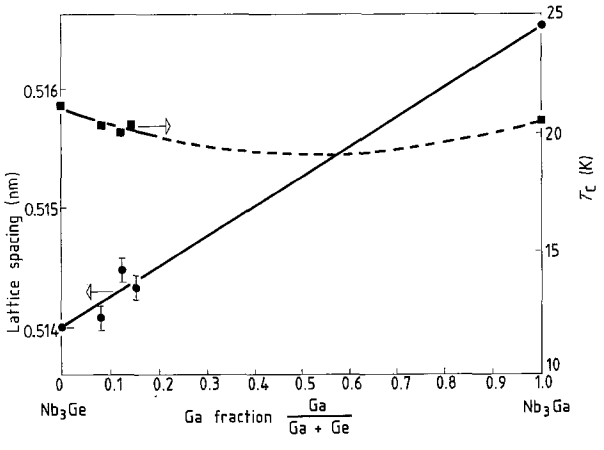

Figure 17 Lattice spacing and T_c for stoichiometric $Nb_3(Ge_xGa_{1-x})$ plotted against x [48].

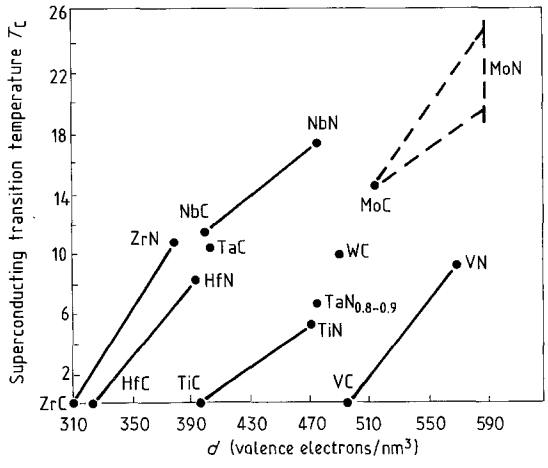

Figure 19 The T_c of B1-type transition-metal carbides and nitrides plotted against valence electron density $d(= n/a_0^3)$, n = number of valence electrons/cell, a_0 = lattice parameter [82].

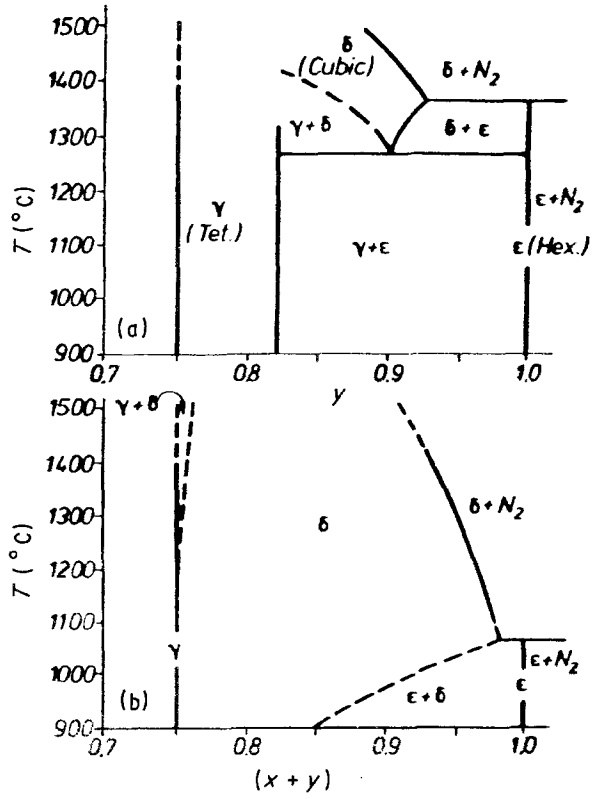

Figure 20 Phase diagram of the system NbC_xN_y [90–93]. (a) $x = 0$, (b) $x = 0.5$. δ, B1-structure; NaCl-type; ε hexagonal, TiP-Type; β, hexagonal, W_2C-type; γ tetragonal.

$P_{tot} = 500\,Pa$; Fibre bundle velocity, $v = 6\,cm\,min^{-1}$; quartz tube diameter 3 cm; length of the reactors 60 cm, temperature-constant zone at 960 ± 20° C: $l \cong 18$ cm; length of the whole deposition apparatus, 3 m; carbon fibre type, PAN-based (7 μm, 1000 to 6000 fibres) Toray, type T300. Only parameters which differ from these values are mentioned below. The reaction gas could be doped with H_2O and $SiCl_4$ [109]. In addition a glow discharge [108] could be ignited.

Fig. 22 shows the deposition rate plotted against the reciprocal absolute deposition temperature $1/T_2$. The deposition rate has the typical dependence that can be expected from CVD processes: at low temperatures there exists a strongly temperature-dependent range in which the deposition is controlled by chemical reactions. At high temperatures the deposition rate decreases with increasing temperature due to homogeneous nucleation in the gas phase. Fig. 22 also shows the grain size, d_g, of the layer, determined from scanning electron micrographs. A grain size of about 100 nm was obtained at a layer thickness of about 0.5 μm. The transition temperature, T_c, of all coatings was in the range 16 to 17 K. The critical current densities, however, show a very strong dependence on the layer thickness as shown in Fig. 23. The current densities were measured on short samples (5 cm length). The reason for the thickness dependence is the coarsening of the grains with increasing layer thickness as shown in Fig. 24. This coarsening, and the decrease in critical current density with increasing layer thickness is well known from the Nb_3Ge deposition [64, 65] and from the sputtering of B1-niobium nitride [100]. The coarsening is caused by the formation of columnar structures with the axis of the columns perpendicular to the substrate.

In order to increase the critical current density, the deposition conditions must be changed by further measures which improve the pinning behaviour of the coating, e.g. by inclusion of pores, grain boundaries and precipitates. The development proceeded in the two steps: (1) development of superconducting thin layers ($d_c \leqslant 100$ nm), and (2) increase of the layer thickness to $d_c \simeq 1$ μm. This thickness is necessary in order to obtain sufficient overall current densities on a 7 μm diameter fibre. In the following sections the different methods of increasing the critical current densities are discussed and compared.

3.2.3. Optimization of the microstructure of thin films ($d_c \leqslant 100$ nm)

3.2.3.1. Refining the microstructure by plasma-enhanced CVD. Plasma-assisted CVD processes are mainly used for deposition at lower temperatures and/or to deposit thermodynamically unstable materials [17]. The plasma-assisted CVD processes can produce amorphous layers as, for example, amorphous silicon for solar cells. Therefore, it was suggested that a gas discharge may change the structure of the B1-NbC_xN_y coating. The inductively or capacitively (Fig. 21)

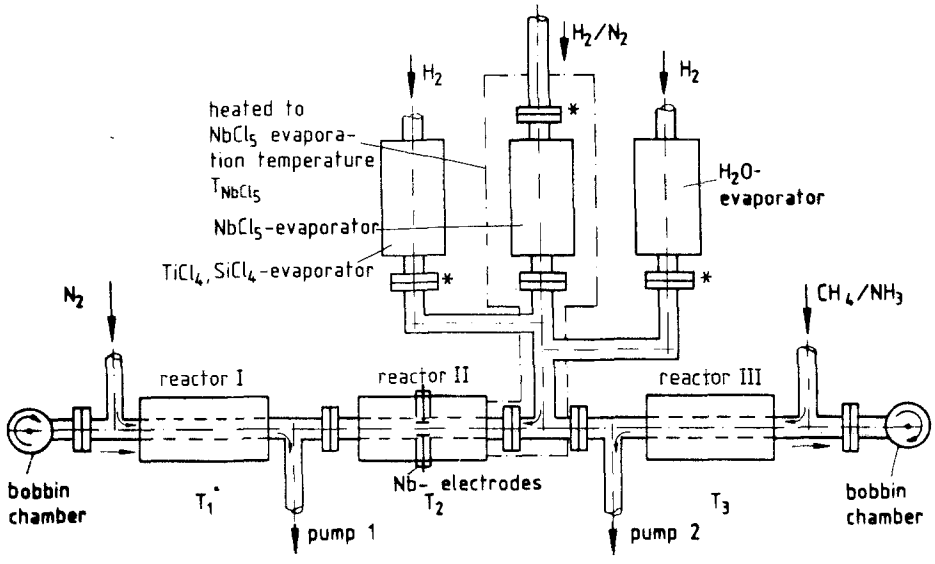

Figure 21 CVD apparatus for B1-NbC_xN_y deposition [108, 109]. The pressure is reduced from atmospheric pressure to the working pressure in the CVD apparatus at the valves indicated by a star.

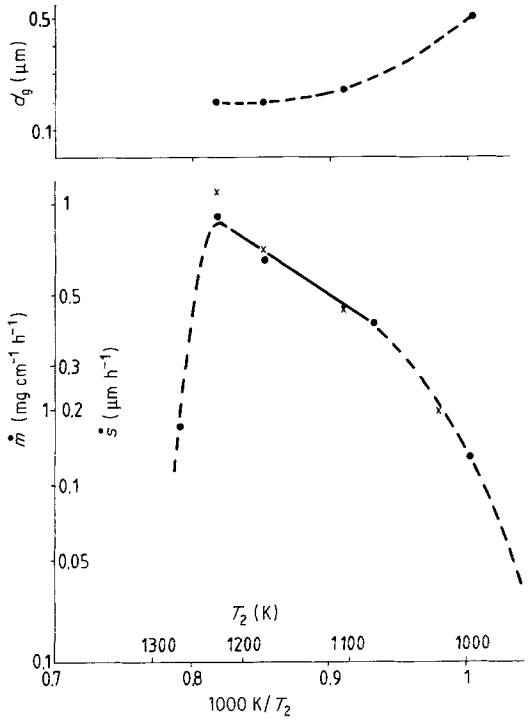

Figure 22 Deposition rate on the bundle (3000 fibres) and grain size d_g plotted against the reciprocal deposition temperature $1/T_2$ [10]. P_{tot} = 5 mbar, 75% H_2, 25% N_2; T_{NbCl_5} = 100° C; V = 6 cm min^{-1}; (●) stationary.

coupled glow discharge (13.56 MHz, 100 W) was ignited in a hot-wall reactor [10, 108].

As shown in Fig. 25, the deposition at lower temperatures ($T_2 \leqslant 900$ K) is possible in the case of a glow discharge. At higher temperatures ($T_2 \geqslant 1000$ K) the deposition is only slightly increased by the glow discharge. The grain size could be reduced in any case (Fig. 26) [108].

3.2.3.2. Refining the microstructure by an ultrasonic field. Ultrasonic fields were used to refine the grain structure of TiB_2 as was demonstrated by Takahashi and Itoh [110]. The influence of an ultrasonic field on the deposition of B1-NbC_xN_y was investigated in a hot-wall tube reactor. The ultrasonic field was excited by a piezo-crystal (20 kHz) at one end of the quartz tube (length 50 cm). The sound pressure level was measured at the other end. The fibre was not moved during the deposition. A grain refinement of a factor

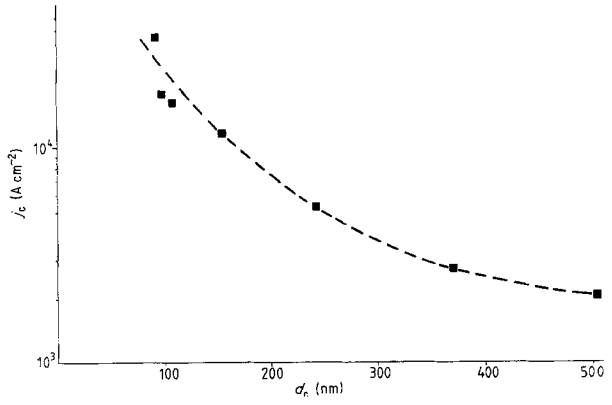

Figure 23 Thickness dependence of the critical current density at T = 4.2 K and B = 7 T [10].

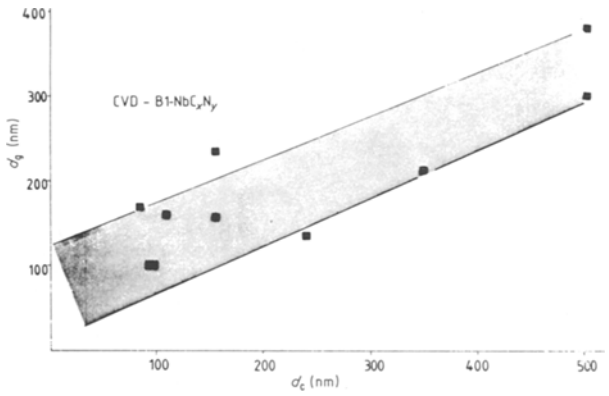

Figure 24 Dependence of mean grain size d_g on the layer thickness d_c.

of approximately 5 [108, 111] was found between a sound pressure level of 1 and 20 dB [108, 111].

3.2.3.3. Optimization of the microstructure by doping of the reaction gas. Doping can have two effects.

1. By changing the surface or the grain-boundary diffusion different nucleation conditions can be achieved.

2. Formation of additional phases and/or changing the composition of the grains.

The influence of H_2O, $SiCl_4$ on the B1-NbC_xN_y deposition has been investigated [109]. H_2O was evaporated in the temperature range $-30° C \leqslant T(H_2O) \leqslant 40° C$, causing the mole fraction of H_2O in the reactor (P_{tot} = 500 Pa) to vary between 0.05% and 10%. Fig. 27 shows that H_2O does not influence the deposition rate, whereas the critical current density at 13 T increases with increasing H_2O content to a maximum value of $j_c \simeq 8 \times 10^3$ A cm^{-2} (Fig. 28). At a higher H_2O content (Figs 28, 29) the B1-NbC_xN_y coating was strongly disturbed, probably caused by internal stresses in the coatings, producing microcracks.

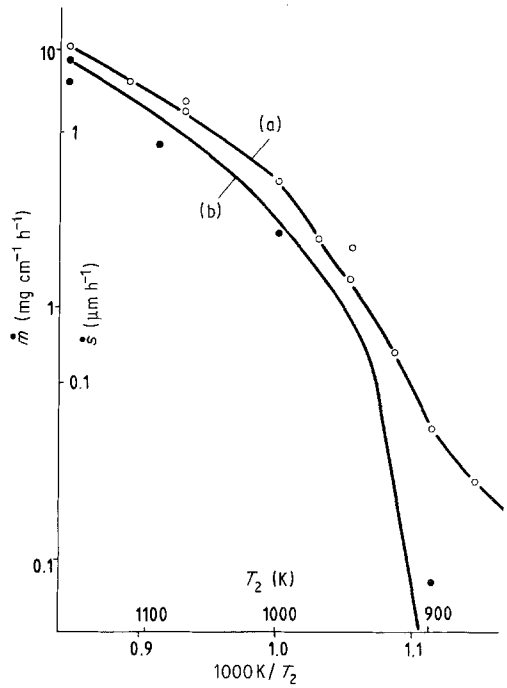

Figure 25 Deposition rate plotted against the temperature (a) with and (b) without glow discharge [10, 108]. P_{tot} = 0.8 mbar, V = 6 cm min^{-1}, ν = 13.56 MHz.

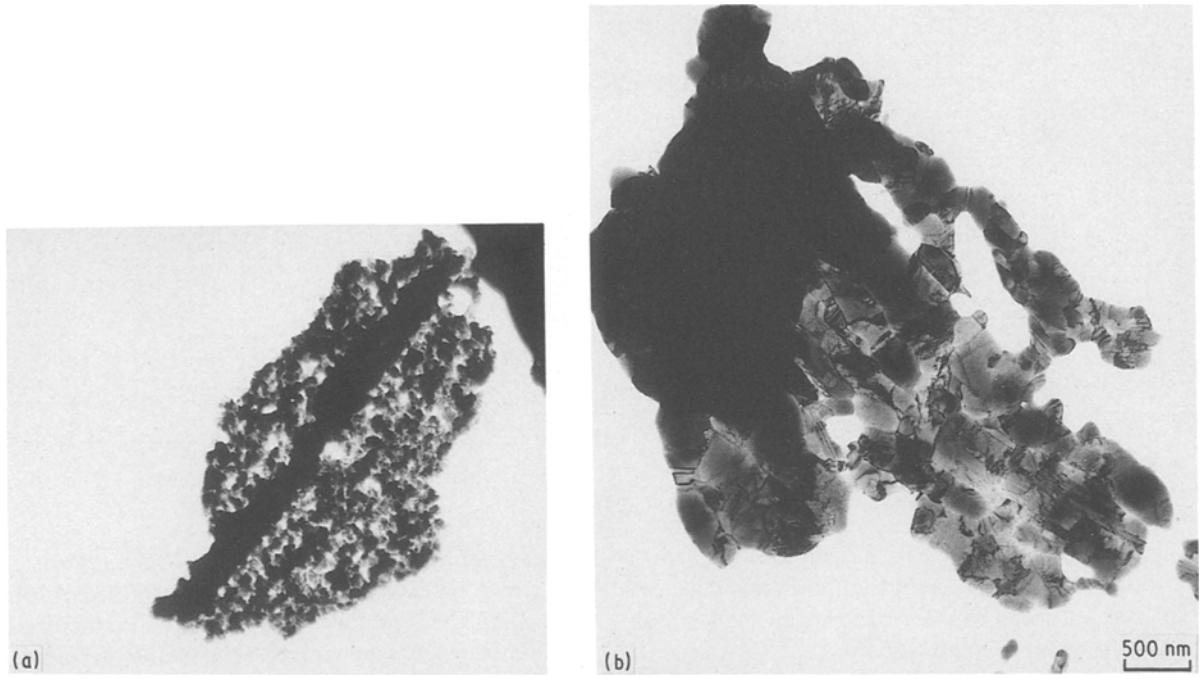

Figure 26 Grain structure (a) with and (b) without gas discharge (TEM pictures) [10]; deposition conditions as mentioned in Section 3.2.2.

The NbC_xN_y coatings produced in the presence of water vapour were investigated by ESCA and X-ray analysis. The ESCA investigations showed no increased oxygen content in the layers deposited from H_2O-containing reaction gases. The X-ray analysis showed, however, a finer grain structure in the presence of water vapour. Therefore, the main reason for the increasing current density seems to be the increasing number of grain boundaries which are effective as pinning centres.

A further increase of j_c can be achieved by $SiCl_4$ additions. Fig. 30 shows the current density at 13 T for different $SiCl_4$ contents in the gas phase.

With increasing $SiCl_4$ content, the current density rises, reaching a maximum at $\sim 3 \times 10^4$ A cm^{-2}. At higher $SiCl_4$ contents, the current density decreases again, probably due to the formation of too much Nb_5Si_3 which reduces the superconducting cross-section. The current density calculated with the total layer thickness therefore decreases. The cross-section effect can be eliminated by plotting the ratio j_c (13 T)/j_c (3T) against the $SiCl_4$ content (Fig. 31). This ratio increases without reaching a maximum.

3.2.3.4. Precipitation of other Nb–C–N phases. The precipitation of additional phases of the same multi-component system is another way to increase the critical current. By precipitation of NB_5Ge_3 in the Nb_3Ge matrix the critical current could be increased as mentioned. Hex-NbC_xN_y precipitations were achieved by decreasing the carbonitriding temperature, T_3. But no increasing current density was measured. The increased pinning behaviour is possibly completely compensated by the reduction in cross-section of the superconducting material.

3.2.3.5. Optimization of the superconducting properties by changed surface conditions. The surface properties of carbon fibres depend on the surface treatment and on the fibre type. High-modulus (HM) fibres have a more graphitized surface than high-tensile (HT) fibres which are produced at lower annealing temperatures. All experiments mentioned up to now were carried out on HT fibres, annealed in a nitrogen atmosphere in order to remove the finish (1000° C). With standard conditions (Section 3.2.2) layers could not be produced on HM fibres due to the more inert chemical properties of the surface (Fig. 32).

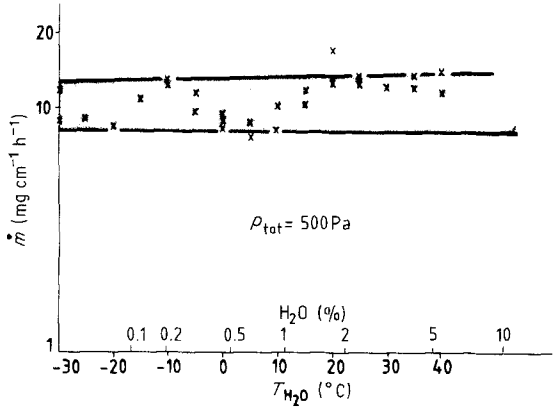

Figure 27 Bl–NbC_xN_y deposition rate plotted against H_2O evaporation temperature and the H_2O mole fraction in the reaction gas [10, 109]. P_{tot} = 500 Pa.

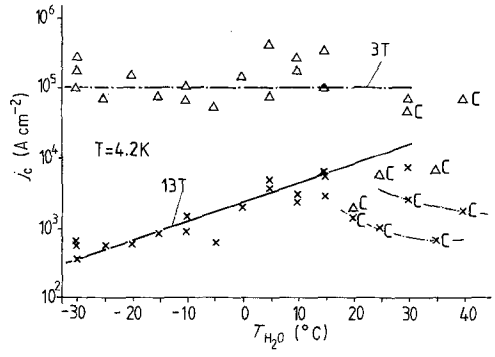

Figure 28 Critical current density j_c at 3 and 13 T plotted against H_2O evaporation. C = Crack formation [10, 109] in the superconductive layer. T = 4.2 K.

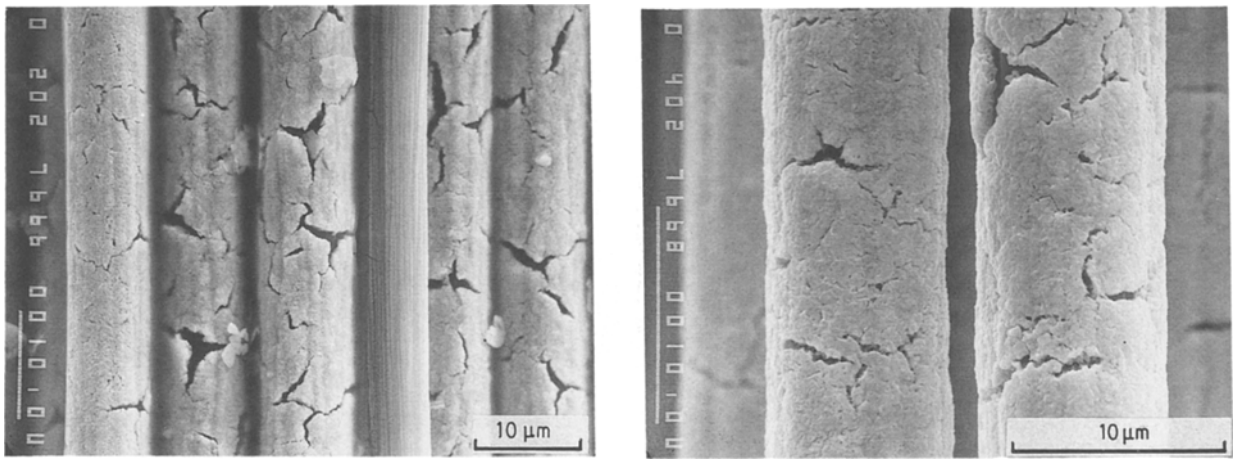

Figure 29 Scanning electron micrograph surface pictures of NbC_xN_y coatings deposited with high T_{H_2O} = 30° C, d_c = 113 nm [10, 109]. An "ideal" coating without any cracks is shown in Fig. 32a.

Another possible surface modification is the deposition of an interlayer between the fibre and the superconductor, in order to influence the nucleation conditions. In addition such an interlayer can seal the carbon fibre against the reaction with the carbonitriding gas (NH_3, CH_4) [112] which can disturb the adhesion by hydrocarbon formation. Two types of coatings were investigated: SiC [112] and tungsten [113] interlayers deposited according to the reactions

$$CH_3SiCl_3 + Ar/H_2 \xrightarrow{800 \text{ to } 1000^\circ C} SiC + \ldots$$

$$WF_6 + 3\,H_2 \xrightarrow{300 \text{ to } 500^\circ C} W + \ldots$$

The deposition apparatus is similar to that shown in Fig. 21, but only with one furnace. The processes were carried out at atmospheric pressure. Both SiC and tungsten interlayers showed the effect of increasing the current densities [112, 113].

W interlayers between the carbon fibre and the B1-NbC_xN_y coatings, generate the highest current densities [113] reached by CVD (Fig. 33). The NbC_xN_y was produced by atmospheric pressure CVD by Brennfleck and co-workers [105 106, 113]. The grain structure in comparison to other coatings is illustrated in Fig. 33, showing in addition that the grain structure of the sputtered coatings of Gavaler *et al.* [100] were almost reached. Fig. 33 shows the expected strong correlation between grain size and critical current.

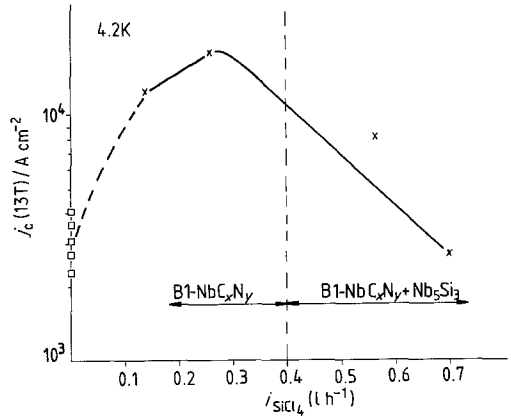

Figure 30 Critical current density at 13 T plotted against $SiCl_4$ gas flow, T_{H_2O} = 15° C [10, 109]. Other deposition conditions as in Section 3.2.2.

3.2.4. Methods of producing thick layers

In order to achieve high overall current densities, a total thickness of about 1 µm on 7 µm diameter fibres is necessary. By using interlayers, further grain growth can be avoided as was shown in the Case of Nb_3Ge coatings (see section 3). First experiments with tungsten interlayers show that the layers interrupt the grain growth of B1-NbC_xN_y with the result that the current increases in proportion to the thickness [112].

3.2.5. Stabilizer material

For electrical and thermal stabilization, a further layer of material with good electrical and thermal properties must be present on the superconducting layer (Section 1). Aluminium is a metal that has suitable properties and can be deposited [114] from the metallorganic compound triisobutylaluminium $[(CH_3)_2CH\text{-}CH_2]_3Al$, which decomposes at temperatures of $T \simeq 250^\circ$ C to aluminium (Fig. 34). Another possibility is the deposition of Cu by an electroless deposition process [115].

3.2.6. Discussion and conclusions

Fig. 35 shows the superconducting properties of the NbC_xN_y coatings discussed so far. Typical values of Nb_3Sn and NbTi are included for comparison [114]. The j_c values for $B \geqslant 13$ T were extrapolated by the Kramer plot [116]. This figure shows the progress which has been made with CVD B1-NbC_xN_y: (1) in an increase of the critical magnetic field at 4.2 K to B_{c2} = 20 to 50 T (thickness $d_c \leqslant 100$ nm); (2) in increasing the critical current densities, e.g. at B = 13 T to 2 × 10^5 A cm^{-2} (thickness $d_c \leqslant 100$ nm).

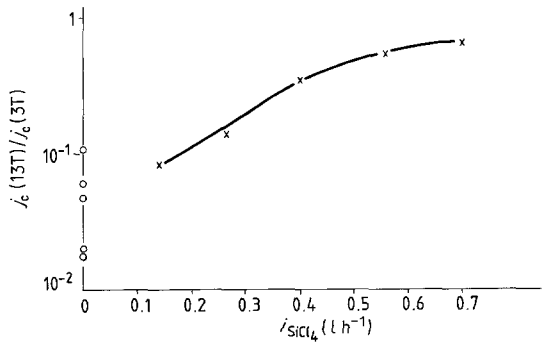

Figure 31 j_c (13 T)/j_c (3 T) plotted against $SiCl_4$ gas flow.

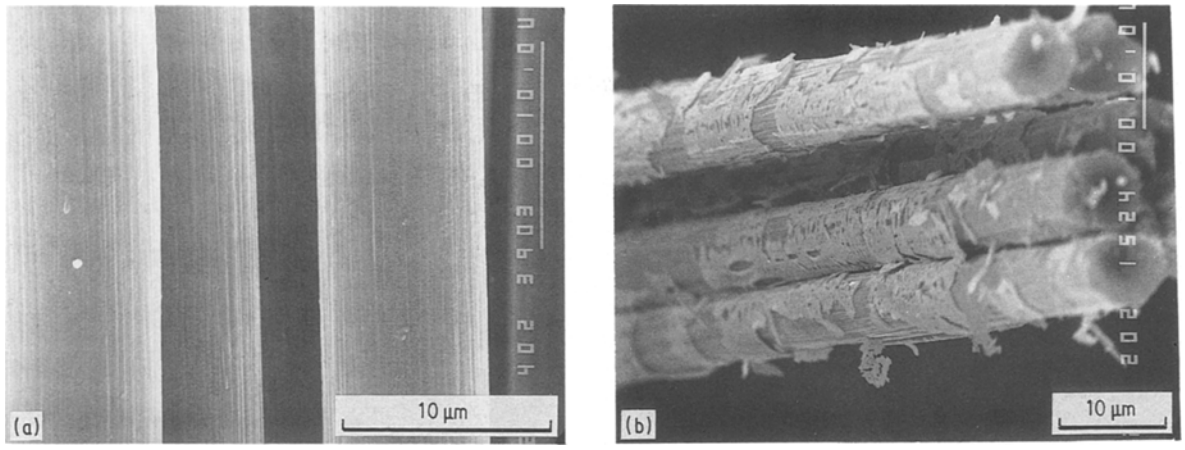

Figure 32 Comparison of a B1-NbC_xN_y layer on (a) HT and (b) HM fibres [10]; deposition conditions as in Section 3.2.2. $T_{H_2O} = 15°C$, $i_{SiCl_4} = 0.3 l h^{-1}$.

The most suitable process for production seems to be CVD with addition of dopants. The chemical engineering of such a process is simple and the production costs are expected to be lower than glow discharge equipment. The maximum length of fibre which produced until now was 100 m. Coils with 2 m carbon fibres were produced with a critical current carrying ability of approximately 100% of the short-sample values. The thickness of the coating and the handling of the carbon fibres must, however, be further optimized.

4. Future developments

CVD processes have the advantage of high deposition rates as was shown in the case of Nb_3Ge, but problems can arise in the production of fine structures because of the high deposition temperatures. This was the case in NbC_xN_y deposition. The advantage is the very high throwing power of this technique.

A new challenge for CVD is the deposition of the new high-temperature superconductors, e.g. $Y_1Ba_2Cu_3O_x$. CVD would have the advantage to deposit on fibres, to deposit preferential orientations and CVD is a process which produces very small radiation damage of the coatings. Both are important because of the high anisotropy of the superconducting properties and the sensitivity of this high-T_c superconductor against radiation. First deposition experiments of superconducting $Y_4Ba_2Cu_3O_x$ were reported recently [117, 118, 119, 120].

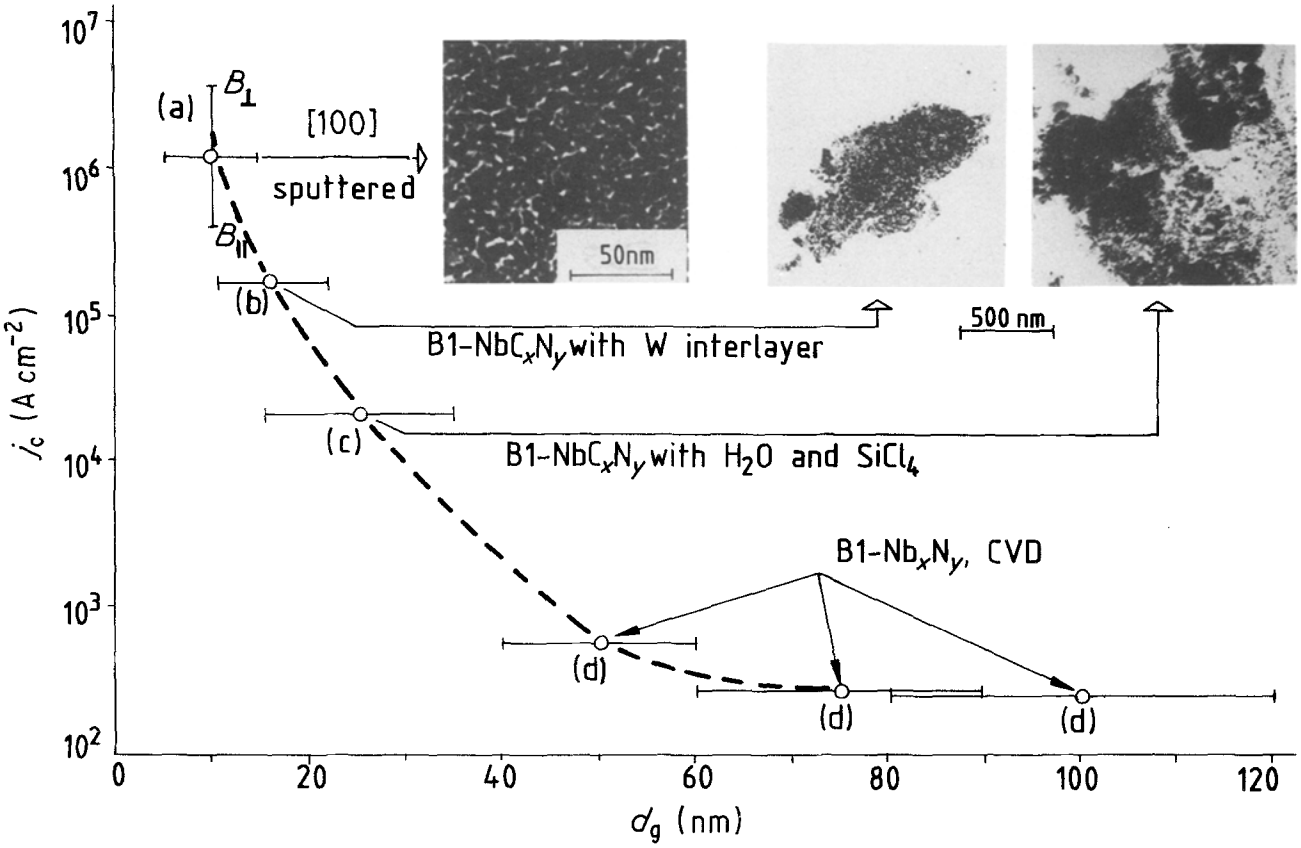

Figure 33 Critical currents plotted against mean grain size d_g, $B = 13$ T, $T = 4.2$ K [10]. (a) Sputtered layer 50 nm, Gavaler *et al.* [100]. (b) NbC_xN_y with tungsten interlayer, $d_c \sim 50$ nm (Section 3.2.2.5). (c) Optimized B1-NbC_xN_y with iCl_4 and H_2O addition, $d_c = 100$ nm (Section 3.2.2.3). (d) B1-NbC_xN_y produced by CVD without additions (Section 3.2.1).

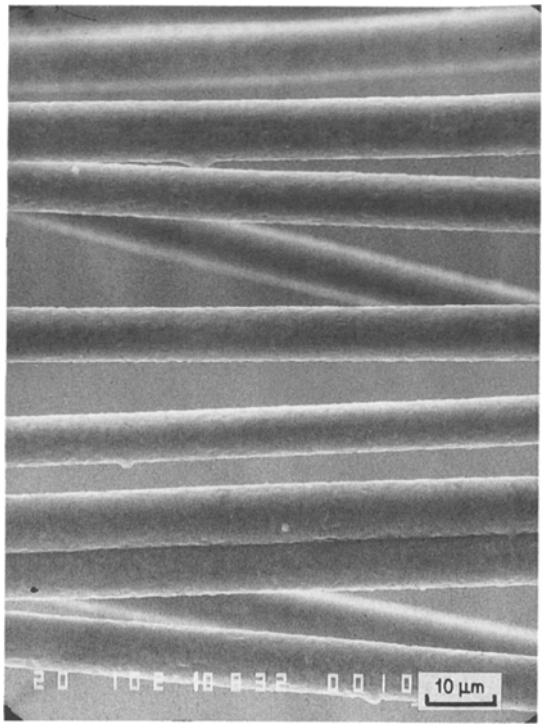

Figure 34 Aluminium-coated carbon fibre.

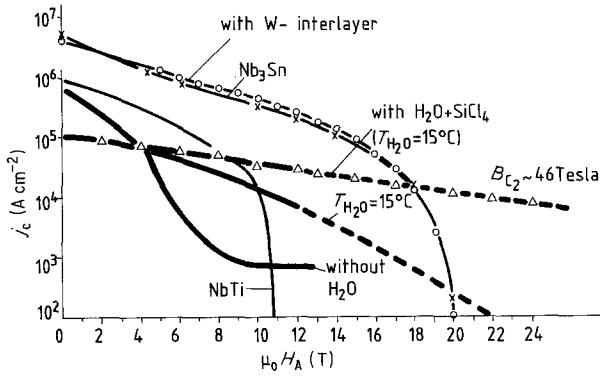

Figure 35 Critical current densities j_c plotted against magnetic field.

Acknowledgement

Part of this paper, concerning NbC_xN_y deposition, was originally published in the Proceedings of the Memorial Seminar of the 20th Anniversary of the Foundation of the Basis Science Division at the Ceramic Society of Japan, "Ceramics: Today and Tomorrow", edited by Sh. Naka, N. Soga, Sh. Kume, Tokyo, 1986. Part of this work was supported by the German Ministry of Research and Technology (BMFT).

References

1. W. HEINZ, *IEEE Trans. Magn.* **Mag. 19** (1983) 167.
2. G. GAMOTA, *ibid. Mag.* **17** (1981) 19.
3. J. G. BEDNORZ and K. A. MÜLLER, *Z. Phys. B* **64** (1986) 189.
4. M. K. WU, J. R. ASHBURN, C. J. TORNG, P. H. HOV, R. L. MENG, L. GAO, Z. J. HUANG Y. Q. WANG and C. W. CHU, *Phys. Rev. Lett.* **58** (1987) 908.
5. Proceedings of the Conference on Low Temperature Physics, *Jpn J. Appl. Phys.* **26** (1987) Suppl. 26–3.
6. K. OKUDA, S. NOGUDI, A. YAMAGISHI, K. SUGIYAMA and M. DATE, *ibid.*, p. 1171.
7. D. DEW-HUGHES, in "Treatise on Materials Science Technoloty", Vol. 14, "Metallurgy of Superconducting Materials," edited by Th. Luhman and D. Dew-Hughes (Academic, New York, 1979) p. 137.
8. D. DEW HUGHES and Th. LUHMAN (eds), *ibid.*, p. 427.
9. O. HENKEL and E. M. SAWITZKY,, "Supraleitende Werkstoffe" (VEB-Verlag fur Grundstoffindustrie, Leipzig, 1982) p. 128.
10. G. WAHL and F. SCHMADERER, in "Ceramics, Today and Tomorrow", edited by Sh. Naka, N. Soga and Sh. Kume (The Ceramic Society of Japan, Tokyo, 1986) p. 165.
11. K. NOTO, in Proceedings 9th International Conference on Magnet Technology, edited by C. Marinucci, P. Weymuth, Swiss Inst. for Nuclear Research (SIN) at ETH-Zürich, Zürich (1985) p. 199.
12. J. R. GAVALER, *J. Vac. Sci. Technol.* **18** (1981) 247.
13. J. D. LIVINGSTON, *Phys. Status Solidi (A)* **44** (1977) 295.
14. M. N. WILSON, in "Superconducting Materials Science, Metallurgy, Fabrication and Application", edited by S. Foner and B. B. Schwartz (Plenum, New York, 1981) p. 63.
15. R. A. BUHRMAN, *Physica* **126B** (1984) 62.
16. W. BUCKEL, "Supraleitung" (Verlag Chemie, Weinheim, 1984).
17. R. F. BUNSHAH, J. M BLOCHER, Th. D. BONFIELD, J. G. FISH, P. B. GHATE, B. E. JACOBSON, D. M. MATTOX, G. E. McGUIRE, M. SCHWARTZ, J. A. THORNTON and R. C. TUCKER, "Deposition Technologies for Films and Coatings" (Noyes Publications, Park Ridge, N.J., 1982).
18. C. F. POWELL, J. H. OXLEY and J. M. BLOCHER, "Vapor Deposition" (Wiley, New York, 1966).
19. Last Conference: Proceedings of the International CVD Conference, X, edited by G. W. Cullen (The Electrochemical Society, Pennington, N.J., 1987).
20. Proceedings of the European CVD-Conferences, Last CVD-Conference Proceedings of Euro CVD VI, edited by R. Porat (Iscar Ltd., Israel, 1987).
21. M. J. HOWES and D. V. MORGAN (eds), "Gallium Arsenide: Materials, Devices and Circuits" (Wiley, Chichester, 1985).
22. J. B. MULLINS, S. J. C. IRVINE, R. H. MOSS, P. N. ROBSON and O. R. WRIGHT, "Metallorganic Vapour Phase Epitaxy 1984", Proceedings the 2nd International Conference on MOCVD 1984, *J. Cryst. Growth* **68** (1984).
23. M. V. ARDENNE, "Tabellen der Elektronenphysik", Vols **I, II** VEB (Deutscher Verlag der Wissenschaften, Berlin, Vol. **I**: 1962; vol. **II**. 1964).
24. G. WAHL, *Thin Solid Films* **40** (1977) 13.
25. G. H. EVANS and R. GREIF, Sandia-Report, SAND (1986) 86-8843.
26. Y. KUSUMOTO, T. HAYASHI and S. KOMIYA, *Jpn J. Appl. Phys.* **24** (1985) 620.
27. C. HOUTMAN, D. B. GRAVES and KI. F. JENSEN, *J. Electrochem. Soc.* **133** (1986) 961.
28. K. CHEN and A. R. MORTAZAVI, *J. Crystal Growth* **77** (1986) 199.
29. G. WAHL, F. SCHMADERER, R. HUBER and R. WEBER, Proceedings VI Euro CVD-Conference, edited by R. Porat (Iscar Ltd., Israel, 1987) p. 176.
30. G. WAHL and P. BATZIES, Proceedings IVth International CVD-Conference, edited by G. F. Wakefield, M. Blocher (ECS, Princeton, 1973) p. 425.
31. E. A. MOELWYN-HUGHES, "Physical Chemistry" (Pergamon, Oxford, 1961).
32. A. N. NESMEYANOV, "Vapor Pressure of the Chemical Elements" (Elsevier, London, 1963).
33. R. HULTGREN, P. DESAI and D. HAWKINS, "Selected Values of the thermodynamic Properties of the Elements" (ASM, Metals Park, Ohio, 1973).
34. E. J. CUKAUSKAS, R. T. HOLM, A. D. BERRY and R. KAPLAN, Appl. Superconductivity Conference,

Baltimore, Maryland 9/28-103 (1986).
E. J. CUKAUSKAS, R. T. HOLM, A. D. BERRY, R. KAPLAN and M. L. H. GREEN, *IEEE Trans. Magn.* **Mag. 23** (1986) 999.
35. H. PAKRASH, *Prog. Cryst. Growth Charact.* **9** (1984) 325.
36. H. SUHR, Ch. OEHR, H. HOLZSCHUH, F. SCHMADERER, G. WAHL, Th. KRUCK and A. KINNEN, *Physica* **C153–155** (1988) 784.
37. J. J. HANAK, in "Metallurgy of Advanced Electronic Materials", edited by G. E. Brock (Interscience, New York, 1963) p. 161.
38. J. J. HANAK, K. STRATER and G. W. CULLEN, *RCA-Rev.* **XXV** (1964) 342.
39. A. C. PRIOR, *Cryogenics* June (1967) 131.
40. A. ECHARRI and M. SPADONI, *ibid.* (1971) 274.
41. L. J. VIELAND and A. W. WICKLUND, *Phys. Lett.* **49A** (1974) 407.
42. H. KAWAMURA and K. TACHIKAWA, *ibid.* **50A** (1974) 29.
43. A. I. BRAGINSKI and G. W. ROLAND, *Appl. Phys. Lett.* **25** (1974) 762.
44. J. R. GAVALER, *ibid.* **23** (1973) 480.
45. F. WEISS, R. MADAR, J. P. SENATEUR, C. BERNARD and R. FRUCHART, *J. Crystal Growth* **56** (1982) 423.
46. O. DEMOLLIENS, F. WEISS, R. MADAR, J. P. SENATEUR and R. FRUCHART, *Ann. de Chemie Fr.* (1984) 959; O. DEMOLLIENS, Thesis, Institut National Polytechnique de Grenoble (June 1986).
47. I. AHMAD, W. J. HOFFERMANN and D. U. GUBSER, *IEEE Trans. Magn.* **13** (1977) 483.
48. M. P. MALEY, L. R. NEWKIRK, J. D. THOMPSON and F. A. VALENCIA, *IEEE Trans. Magn.* **Mag. 17** (1981) 533.
49. V. CERNUSKO, K. FRÖHLICH, M. JERGEL, D. MACHAJEDIK, M. TARNOVSKA and V. K. FEDOROV, *J. Phys.* **C1** (1984) 429.
50. V. CERNUSKO, K. FRÖHLICH, D. MACHAJDIK and M. JERGEL, *IEEE Trans. Magn.* **Mag. 17** (1981) 2051.
51. A. MÜLLER, *Z. Metallkde* **71** (1980) 507.
52. *Idem,* US Patent, 4 336 280 (1982).
53. L. R. NEWKIRK, F. A. VALENCIA and T. C. WALLACE, *J. Electrochem. Soc.* **123** (1976) 425.
54. F. WEISS, C. BERNARD and R. FRUCHART, Proceedings VIII International CVD Conference 1981, edited by J. Blocher, G. E. Vuillard and G. Wahl (ECS, Pennington, 1981) p. 44.
55. R. MADAR, F. WEISS, R. FRUCHART and C. BERNARD, *J. Crystal Growth* **45** (1978) 37.
56. A. I. BRAGINSKI, M. R. DANIEL and C. W. ROLAND, *AIP Conf. Proc.* **34** (1976) 78.
57. L. LI, B. ZHAO, P. ZHONS, S. GUO and Y. ZHAO, *J. Low Temp. Phys.* **45** (1981) 287.
58. A. I. BRAGINSKI, J. R. GAVALER, G. W. ROLAND, M. R. DANIEL, M. A. JANOCKO and A. A. SANTHANAM, *IEEE Trans. Mag.* **Mag-13** (1977) 300.
59. R. E. ENSTROM, J. J. HANAK and G. W. CULLEN, *RCA Rev.* **31** (1970) 702.
60. R. E. ENSTROM and J. R. APPERT, *J. Appl. Phys.* **43** (1972) 1915.
61. G. ZIEGLER, B. BLOS, H. DIEPERS and K. WOHLLEBEN, *Z. Angew. Phys.* **31** (1971) 184.
62. Y. UZEL and H. DIEPERS, *Z. Phys.* **258** (1973) 126.
63. A. I. BRAGINSKI, G. W. ROLAND, M. R. DANIEL, A. T. SANTHANAM and K. W. GUARDIPEE, *J. Appl. Phys.* **49** (1978) 736.
64. A. I. BRAGINSKI, G. W. ROLAND and A. T. SANTHANAM, *IEEE Trans. Mag.* **Mag-15** (1979) 505.
65. R. T. KAMPWIRTH, *ibid.* **Mag-15** (1979) 502.
66. M. P. MALEY, L. R. NEWKIRK, J. D. THOMPSON and F. A. VALENCIA, Final Report, EPRI-EL 965, Research Project 7855-1 (1979).
67. J. W. EKIN, *J. Appl. Phys.* **54** (1983) 303.
68. J. J. HAUSER and H. C. THEUERER, *Phys. Rev.* **134** (1964) 1A 198.
69. S. A. ALTEROVITZ, E. J. HAUGLAND and J. A. WOOLAM, *Phys. Rev. B* **23** (1981) 4485.
70. I. V. PETRUSEVIC, L. A. NISELSON, F. N. KOZLOV, V. P. BOGOANOV and V. V. ABRAMOV, *Izv. Akad. Nauk SSSR, Metally* **3** (1974) 77.
71. J. J. HAUSER and H. C. THEUERER, *Phys. Rev.* **129** (1963) 103.
72. G. WEBB and J. ENGLEHARDT, *IEEE Trans. Magn.* **Mag-11** (1975) 208.
73. V. M. PAN, V. P. ALEKSEEVSKII, A. G. POPOV, Yu. I. BELETSKII, L. M. YUPKO and V. V. YAROSH, *JETP Lett.* **21** 228 (1975) cited after [8].
74. K. TOGANO, H. KUMAKURA, Y. YOSHIDA and K. TACHIKAWA, *IEEE Trans. Magn.* **Mag-21** (1985) 463.
75. K. INOUE, T. KURODA and K. TACHIKAWA, *ibid.,* **Mag-21** (1985) 467.
76. H. YAMASAKI and Y. KIMURA, *Mat. Res. Bull. Vol.* **21** (1986) 125.
77. T. TOGANO and K. TACHIKAWA, *Adv. in Cryogenic Engineering and Materials* **34** (1987) 451.
78. C. L. H. THIEME, S. POURRAHIMI, B. B. SCHWARTZ and S. FONER, *ibid.,* **44** (1984) 260.
79. M. SUZUKI, T. ANAYAMA, K. WATANABE, N. TOYOTA, N. KOBAYASHI, K. NOTO and Y. MUTO, *Jap. Journ. Appl. Phys.* **24** (1985) L767.
80. A. I. BRAGINSKI, J. R. GAVALER and G. W. ROLAND, *IEEE Trans. Magn.* **Mag-13** (1977) 300.
81. Th. WOLF, Physikalisches Institut der Universität Karlsruhe, Thesis, Karlsruhe (1982).
82. ZHAO YOU-XIAN and HE SHOU-AN, *Solid State Commun.* **45** (1983) 281.
83. G. LINKER, R. SMITHEY and O. MEYER, *J. Phys. F Met. Phys.* **14** (1984) L115.
84. B. M. KLEIN and W. E. PICKET, in "Superconductivity in d- and f-band", edited by W. Buckel and W. Weber (Kernforschungszentrum, Karlsruhe, 1982) p. 477.
85. W. L. McMILLAN, *Phys. Rev.* **167** (1968) 331.
86. B. T. MATTHIAS, E. CORENZWIT, A. S. COOPER and L. O. LONGINOTTI, *Proc. Nat. Acad. Sci.* **68** (1971) 56.
87. D. DEW-HUGHES and R. JONES, *Appl. Phys. Lett.* **36** (1980) 856.
88. J. W. EKIN, *IEEE Trans. Magn.* **Mag-17** (1981) 658.
89. J. W. EKIN, J. R. GAVALER and J. GREGG, *Appl. Phys. Lett.* **41** (1982) 996.
90. E. K. STORMS, *High Temp. Sci.* **7** (1975) 391.
91. *Idem, MTP Int. Rev. Sci.* **10** (1972) 37.
92. R. W. GUARD, J. W. SAVAGE and D. G. SWARTHOUT, *Trans. AIME* **239** (1967) 643.
93. G. E. PIKE, H. O. PIERSON, A. W. MULLENDORE and J. E. SCHIRBER, *Appl. Polym. Symp.* **29** (1976) 71.
94. N. PESSAL and J. K. HULM, *Physics* **2** (1966) 311.
95. J. K. HULM and B. T. MATTHIAS, in "Superconductor Materials Science, Metallurgy, Fabrication and Applications", edited by S. Foner and B. B. Schwarz (Plenum, New York, 1981) p. 1.
96. M. W. WILLIAMS, K. M. RALLS and M. R. PICKUS, *J. Phys. Chem. Sol.* **28** (1967) 333.
97. B. T. MATTHIAS, *Phys. Rev.* **92** (1953) 874.
98. *Idem, ibid.* **97** (1955) 74.
99. J. R. GAVALER, A. I. BRAGINSKI, M. ASHKIN and At. SANTHANAM, in "Superconductivity in d- and f-Band Metals", edited by H. Suhl and M. B. Maple (Academic, New York, 1980) p. 25.
100. J. R. GAVALER, A. T. SANTHANAM, A. I. BRAGINSKI, M. ASHKIN and M. A. ANOCKO, *IEEE Trans. Magn.* **Mag-17** (1981) 573.
101. M. DIETRICH and L. J. PATEROK, *Cryogenics* **24** (1984) 636.
102. W. D. SMITH, R. Y. LIN and J. ECONOMY, *Appl. Polym. Symp.* **29** (1976) 83.
103. J. ECONOMY, R. Y. LIN, W. D. SMITH and C. K.

JUN, Air France Materials Laboratory Report No. AFMLR-TR-72-189 (1972).
104. M. C. OHMER and W. G. D. FREDERICK, *J. Appl. Phys.* **45** (1974) 1382.
105. K. BRENNFLECK, Thesis, Karlsruhe (1982).
106. K. BRENNFLECK, M. DIETRICH, E. FITZER and D. KEHR, Proceedings 7th International CVD Conference, edited by Th. O. Sedgwick and H. Lydtin (ECS, Princeton, 1979) p. 300.
107. M. DIETRICH, K. BRENNFLECK and E. FITZER, Proceedings International CVD Conference, edited by J. M. Blocher, G. E. Vuillard and G. Wahl (ECS, Paris, 1981) p. 759.
108. M. DIETRICH, C. H. DUSTMANN, F. SCHMADERER and G. WAHL, *IEEE Trans. Magn.* **Mag-19** (1983) 406.
109. F. SCHMADERER and G. WAHL, Proceedings Vth Euro CVD Conference on CVD, edited by J. O. Carlson and L. Lindström, (Uppsala Uni., Uppsala, 1985) p. 533.
110. T. TAKAHASHI and H. ITOH, *J. Crystal Growth* **49** (1980) 445.
111. S. BALDUF, Diplomarbeit, Fachhochschule für Technik, Mannheim (1982) available from G. Wahl.
112. K. BRENNFLECK, E. FITZER, G. SCHOCH and M. DIETRICH, Proceedings IXth International CVD Conference, edited by McD. Robinson, C. H. J. v. d. Brekel, G. W. Cullen and J. M. Blocher (ECS, Pennington, 1984) p. 649.
113. K. BRENNFLECK, personal communication (1987).
114. F. SCHMADERER, G. WAHL, M. DIETRICH, Proceedings IXth International CVD-Conference, edited by McD. Robinson, C. H. J. v. d. Brekel, G. W. Cullen, J. M. Blocher, (ECS, Pennington, 1984) p. 663.
115. G. WAHL and F. SCHMADERER, in "Stromlose Beschichtung", edited by A. F. Bogenschütz (Leuze Verlag, Saulgau, 1988) p. 124.
116. E. J. KRAMER, *J. Appl. Phys.* **44** (1973) 1360.
117. H. YAMANE, H. KUROSAWA, H. IWASAKI, H. MASUMOTO, T. HIRAI, N. KOBAYASHI and Y. MUTO, *Jap. Journ. Appl. Phys.* **27** (1988) p. L 1275.
118. T. NAKAMORI, H. ABE, T. KANAMORI and S. SHIBATA, *Jap. Journ. Appl. Phys.* **27** (1988) p. L 1265.
119. A. D. BERRY, D. K. GASKILL, R. T. HOLM, R. KAPLAN and R. L. HENRY, *Appl. Phys. Lett.* **52** (1988) 1743.
120. F. SCHMADERER and G. WAHL, to be published, 1989.

Received 22 September 1987
and accepted 19 May 1988